Journal of Molecular Graphics and Modelling 29 (2010) 331–346

Contents lists available at ScienceDirect

Journal of Molecular Graphics and Modelling

journal homepage: www.elsevier.com/locate/JMGM

Interaction of the disaccharides trehalose and gentiobiose with lipid bilayers: A comparative molecular dynamics study

Bruno A.C. Horta*, Lovorka Perić-Hassler, Philippe H. Hünenberger*

Laboratory of Physical Chemistry, ETH Zürich, CH-8093 Zürich, Switzerland

ARTICLE INFO

Article history:
Received 26 July 2010
Received in revised form
24 September 2010
Accepted 30 September 2010
Available online 8 October 2010

Keywords:
Computer simulation
Molecular dynamics
Disaccharides
Gentiobiose
Trehalose
Lipid bilayer

ABSTRACT

The disaccharide α,α-trehalose (TRH) is known for its bioprotective action in organisms subject to stressful environmental conditions. However, the mechanisms whereby TRH stabilizes biomolecules remains matter of debate, the five main hypotheses being the water replacement (WRH), headgroup bridging (HBH), vitrification (VIH), water entrapment (WEH) and hydration forces (HFH) hypotheses. Four hypotheses (all except HFH) are in principle compatible with a preferential affinity of the sugar molecules (compared to water) for the biomolecular surface. According to the recently proposed sugar-like mechanism (Pereira and Hünenberger [29]), preferential affinity would result from the entropy gain upon releasing many water molecules from the surface region to the bulk, at the cost of immobilizing and rigidifying fewer sugar molecules. Thus, a more flexible disaccharide such as gentiobiose (GNT) should evidence a weaker preferential affinity, limiting its bioprotective ability. In this work, molecular dynamics (MD) simulations of a dipalmitoyl-phosphatidylcholine (DPPC) bilayer patch in the presence of either pure water or aqueous solutions of GNT or TRH are performed in order to assess the validity of this suggestion. At 475 K and 1.6 m (molal), TRH indeed preserves the bilayer structure to a larger extent compared to GNT. However, the present investigation does not unambiguously indicate which of the above mechanism takes place, since the simulations reveal characteristic features of all of them. This suggests either that multiple mechanisms may be simultaneously active or that their definitions are not precise enough.

1. Introduction

Nature has evolved numerous strategies for the long-term survival of organisms exposed to potentially damaging conditions like extreme dryness, cold, heat, pressure, salt concentration, acidity or oxygen deprivation [1,2]. One of these strategies, cryptobiosis, involves a reversible suspension of the metabolism and a temporary effective isolation from the environmental stress [3,4]. Probably the best studied case of cryptobiosis concerns anhydrobiosis, namely the resistance to nearly complete dehydration [1,4–8]. A characteristic feature of the anhydrobiotic process is the accumulation of large amounts of saccharides in the cell [9,10], and in particular of the disaccharide trehalose [5,11] (α,α-trehalose, TRH; Fig. 1).

It is generally accepted that bioprotection involves the stabilization of biomolecules such as proteins [12–18] (against irreversible denaturation) and lipid membranes [7,9,19–26] (against mechanical disruption). A possible stabilization of nucleic acids [27] has also been recently proposed. Five possible mechanisms have been put forward to tentatively explain the bioprotective action of sugars, principally concerning the best documented example of anhydrobiosis [28,29]:

1. The *water replacement hypothesis* (WRH) suggests that during dehydration, sugar molecules can substitute water molecules in forming hydrogen bonds (H-bonds) with the polar and charged groups present at the biomolecular surface, thereby inhibiting the denaturation (proteins) or a transition to the gel phase (membranes) [5,30–40].
2. The *headgroup-bridging hypothesis* (HBH) is an extension of the WRH formulated based on simulations in the context of membrane bioprotection, which proposes that sugar molecules form a scaffold of H-bonds bridging multiple headgroups, thereby inhibiting a transition to the gel phase upon dehydration [29] (this scaffold is labile in the dilute regime [29,41–43] but expected to strengthen upon dehydration, as a result of the removal of the water molecules competing for the headgroup H-bonding sites and of the reduction of dielectric screening effects).

* Corresponding authors at: ETH Zürich, Laboratorium für Physikalische Chemie, ETH–Hönggerberg, HCI, CH-8093 Zürich, Switzerland. Tel.: +41 44 632 5503; fax: + 41 44 632 1039.
E-mail addresses: bruno.horta@gmail.com (B.A.C. Horta), phil@igc.phys.chem.ethz.ch (P.H. Hünenberger).

1093-3263/$ – see front matter © 2010 Elsevier Inc. All rights reserved.
doi:10.1016/j.jmgm.2010.09.013

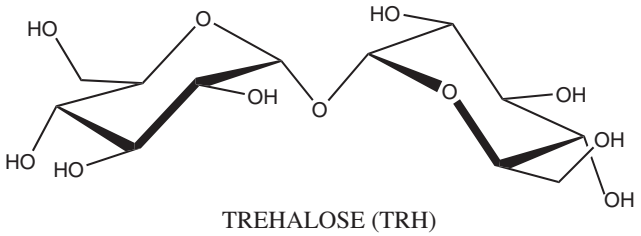

TREHALOSE (TRH)

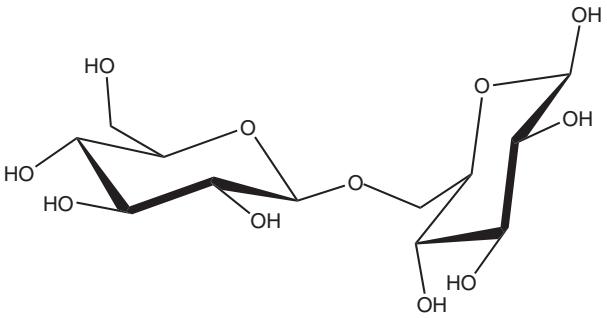

GENTIOBIOSE (GNT)

Fig. 1. Structures of the two disaccharides considered in the present study. Trehalose (α,α-trehalose, TRH; Glcα (1→1)αGlc) is the non-reducing disaccharide consisting of two D-glucopyranose (Glc) residues in a α (1→1)α (two-bond, axial–axial) glycosidic linkage. Gentiobiose (GNT; represented here in its β-anomeric form at the reducing residue; Glcβ(1→6)Glcβ) is the reducing disaccharide consisting of two Glc residues in a β(1→6) (three-bond, equatorial–equatorial) glycosidic linkage.

3. The *vitrification hypothesis* (VIH) suggests that sugars found in anhydrobiotic systems, known to be good vitrifying agents, protect biomolecules through the formation of amorphous glasses, thereby reducing structural fluctuations and preventing denaturation (proteins) or mechanical disruption (membranes) [44–50].
4. The *water-entrapment hypothesis* (WEH) proposes that sugars concentrate residual water molecules close to the biomolecular surface, thereby preserving to a large extent its solvation and native properties in the quasi-dry state [51–57].
5. The *hydration forces hypothesis* (HFH), introduced more recently in the context of membrane bioprotection, proposes that sugar molecules are preferentially excluded from the biomolecular surface [58,59], and indirectly reduce the compressive stress in the membrane upon dehydration ("hydration repulsion" between bilayers brought in contact), thereby preventing a transition to the gel phase [58,60].

Note that these mechanisms are not necessarily all mutually exclusive. For example, the WRH and the VIH are often invoked simultaneously to explain the bioprotective effect of sugars against dehydration [4,9,10,34,49,61]. Since there is experimental or/and theoretical evidence supporting each of the five above hypotheses in specific situations, it is not impossible that the bioprotection mechanism varies depending on the nature of the environmental stress and its intensity, as well as on the type of protected biomolecule.

Recent molecular dynamics (MD) simulation studies indeed suggested that there is a qualitative difference in the way sugars interact with membranes and with proteins [62]. In the case of membranes, the simulations [29,41–43,63–72] systematically revealed a preferential affinity of the sugar molecules for the bilayer surface and a direct interaction (through H-bonds) with the lipid headgroups, even in dilute solutions, providing support for the WRH (possibly along with [29,41–43] the HBH). In contrast, in the case of proteins, the simulations [51,53,57,54,56,73–77] rather suggested a preferential exclusion of the sugar molecules from the biomolecular surface (trapped water layer), even in concentrated solutions, providing support for the WEH (along with the VIH for concentrated sugar solutions [74]).

Closely related to the question of the bioprotection mechanism is that of the particular efficiency of TRH (compared to, e.g. other disaccharides or oligosaccharides) in terms of bioprotective action. TRH is the non-reducing disaccharide composed of two D-glucopyranose units in an (axial–axial) $\alpha(1 \rightarrow 1)\alpha$-linkage. Recent MD simulation studies of the 11 glucose-based disaccharides in water [78] (see also Refs. [79,80]) have revealed two peculiar features of TRH which, in combination, confer to this compound rather unique properties in the series, namely a high conformational rigidity (low conformational entropy) and the absence of significant intramolecular H-bonding (suggesting a high propensity to intermolecular H-bonded interactions). In pictorial terms, TRH could thus be viewed as a kind of "hydroxyl porcupine", presenting a high density of molecular hydroxyl groups in essentially fixed relative positions and orientations, and exempt of intramolecular H-bonding interactions (i.e. available for intermolecular interactions with the solvent, with other sugar molecules or with biomolecules).

In a recent study, Pereira and Hünenberger [29] proposed (based on MD simulations and available experimental data) two mechanisms for the interaction of polyhydroxylated cosolutes with lipid bilayers. The *alcohol-like mechanism* (active for small alcohols and polyols) involves preferential affinity of the cosolute (compared to water) for the superficial region of the bilayer interior, and is driven by the hydrophobic effect. It results in a lateral expansion of the membrane, a disorder increase within the bilayer, and a partial substitution of water by cosolute molecules at the H-bonding sites provided by the membrane (predominantly at the level of the ester groups). The *sugar-like mechanism* (active for larger polyols including saccharides; see also Ref. [62]) involves preferential affinity of the cosolute (compared to water) for the bilayer surface and is mainly driven by entropic effects. It results in the absence of lateral expansion and change in disorder within the bilayer, and in a partial substitution of water by cosolute molecules at the H-bonding sites provided by the membrane (predominantly at the level of the phosphate groups). It also involves the clustering of the cosolute molecules at the membrane surface (formation of a coating layer) and the bridging of lipid molecules *via* H-bonded cosolute molecules. H-bonding itself is not viewed as a driving force for these two mechanisms, which only involve the (partial) substitution of water-lipid by cosolute-lipid H-bonds (the sum of the two remaining essentially constant, irrespective of the nature and concentration of the cosolute).

If one accepts the sugar-like mechanism, which is compatible with the WRH, HBH, VIH and possibly WEH (but not with the HFH), as providing an essentially correct description of sugar–membrane interactions, the main driving force for the clustering of sugar molecules at the bilayer surface is the release of many water molecules from the surface region to the bulk (large entropy increase) at the cost of immobilizing and rigidifying much fewer (already inherently rather rigid) sugar molecules in this same region (limited entropy cost), the process being enthalpically essentially neutral (exchange of H-bonding partners for the lipid headgroups). In this case, the particularly strong bioprotective capacity of TRH could be in large part a consequence of its very limited conformational flexibility in solution (low entropy cost of rigidification), secondary factors [19,20,81] being a favorable hydroxyl group disposition [82,83] (to interact with a planar surface), a strong propensity to self-aggregate [84,85], strong kosmotropic properties [86–94], an elevated glass transition tem-

perature [81,95] (contribution of the VIH), a high chemical stability [81] (against acidic or enzymatic hydrolysis) and an antioxidant activity [96,97].

If the above reasoning is correct, a more flexible disaccharide should evidence a reduced preferential affinity and a more limited bioprotective ability for lipid bilayers compared to TRH. Recent MD simulations of the 11 glucose-based disaccharides in water [78] (see also Refs. [79,80]) suggested that the $\beta(1 \rightarrow 6)$-linked disaccharide gentiobiose (GNT; Fig. 1), which has one additional torsional degree of freedom in its glycosidic linkage, is, at the opposite of TRH, the most flexible (highest entropy) compound in the series. This observation is also corroborated by other experimental and theoretical studies [79,80,98–100]. However, like TRH, GNT does not present persistent intramolecular H-bonds in aqueous solution. As a consequence, the hydroxyl groups of the two molecules are engaged to a similar extent in interactions with water in the dilute regime, and *a priori* similarly prone to intermolecular interaction in the more concentrated regime or in the presence of a lipid bilayer. Therefore, a comparison of TRH and GNT in terms of their interaction with membranes appears to represent an interesting test for the above ideas.

In the present work, explicit-solvent MD simulations of a dipalmitoyl-phosphatidylcholine (DPPC) bilayer patch in the presence of pure water or of aqueous solutions of the two disaccharides are reported and compared, in order to investigate the effect of the difference in flexibility between the two sugars on their interaction with the bilayer (and the resulting alteration of the bilayer properties), and on their potential for bioprotection. To this purpose, a total of 20 simulations (10 ns each) have been carried out, differing in the thermodynamic ensemble considered (simulations either at constant lateral area and normal pressure or at constant pressure), disaccharide identity and concentration (pure water, GNT or TRH at either 0.8 or 1.6 m concentration, "m" indicating the solution molality in mol kg^{-1}) and temperature (323 or 475 K).

2. Computational details

2.1. Molecular dynamics simulations

All MD simulations were performed using the GROMOS96 program [101,102] together with the GROMOS 45A4 force-field [103–107] (including recently reoptimized parameter sets for lipids [106] and carbohydrates [79,80,103,108,109]) and the SPC water model [110]. The simulations were carried out under periodic boundary conditions based on rectangular boxes containing a DPPC lipid bilayer patch of $2 \times 6 \times 6$ lipid molecules (in the *xy*-plane, i.e. normal to the *z*-axis) in the presence of either pure water or a disaccharide (GNT or TRH) solution (Section 2.2). Newton's equations of motion were integrated using the leap-frog scheme [111] with a timestep of 2 fs. All bond lengths were constrained using the SHAKE procedure [112] with a relative geometric tolerance of 10^{-4}. The center of mass motion was removed every 100 ps. The simulations were performed in two different thermodynamic ensembles: (i) the $NA_{xy}P_zT$ ensemble (constant number of particles N, area in the *xy*-plane A_{xy}, pressure along the *z*-axis P_z, and temperature T), with $P_z = 1$ bar, $T = 323$ or 475 K, and $A_{xy} = 23.04\ nm^2$, the latter using identical box dimensions along the *x*- and *y*-axes and based on an area per lipid $a_{xy} = 0.64\ nm^2$ (consensus experimental estimate [113] for DPPC in the liquid-crystalline phase at full hydration and at 323 K); (ii) the *NPT* ensemble (constant number of particles N, pressure P, and temperature T), with $P = 1$ bar and $T = 323$ or 475 K using identical (fluctuating) box dimensions along the *x*- and *y*-axes [114]. The temperature was maintained by weakly coupling the solute and solvent degrees of freedom separately to a temperature bath [115] at temperature T, with a relaxation time of 0.1 ps. The pressure was maintained by weakly coupling the particle coordinates and box dimensions to a pressure bath at pressure 1 bar (P_z only in the $NA_{xy}P_zT$ ensemble, P_{xy} and P_z separately [114] in the *NPT* ensemble), with a relaxation time of 0.5 ps and an isothermal compressibility of 4.575×10^{-4} (kJ mol^{-1} $nm^{-3})^{-1}$ [101]. The nonbonded interactions were calculated using a twin-range scheme [101,116], with short- and long-range cutoff distances set to 0.8 and 1.4 nm, respectively, and a frequency of 5 timesteps for the update of the short-range pairlist and intermediate-range interactions. A reaction-field correction [117,118] was applied to account for the mean effect of electrostatic interactions beyond the long-range cutoff distance, using a relative dielectric permittivity of 61 as appropriate for the SPC water model [119]. Configurations were saved every 5 ps for analysis (Section 2.3).

2.2. Molecular systems

The (periodic) DPPC bilayer patch ($2 \times 6 \times 6$ lipid molecules) was simulated in the presence of either pure water or aqueous solutions of the disaccharides GNT or TRH, at different temperatures (323 or 475 K) and concentrations (0.8 or 1.6 m, "m" indicating the solution molality in mol kg^{-1}). The disaccharide GNT was simulated in its β-anomeric form at the reducing residue, expected to account for 61.7% of the total anomeric population [120,121]. The 20 resulting simulations are labelled using a three-letter code: the successive letters refer to the thermodynamic ensemble (A: $NA_{xy}P_zT$ ensemble; P: *NPT* ensemble), nature of the solution environment (W: pure water; G_l and G_h: GNT at 0.8 or 1.6 m; T_l and T_h: TRH at 0.8 or 1.6 m) and temperature (L: lower temperature of 323 K; H: higher temperature of 475 K). The lower temperature of 323 K corresponds to a common choice in experimental studies concerning DPPC bilayers in the liquid-crystalline phase [113]. The higher temperature of 475 K is not meant to represent a physical situation. It is used here (like in previous studies [41,79]) as a mere device to place the bilayer under stress conditions and investigate how the disaccharides affect the response of the membrane. The two considered concentrations were modeled by inclusion of disaccharide molecules in ratios one-to-two (0.8 m; total 36 disaccharide molecules) or one-to-one (1.6 m; total 72 disaccharide molecules) relative to the lipid molecules, and appropriately selecting the corresponding numbers of water molecules (see below).

The initial structure of the DPPC bilayer was constructed by applying 36 lattice translations and random axial rotations to a single pair of tail-to-tail lipid molecules, so as to generate two leaflets of area A_{xy}. The resulting bilayer was solvated using 2166 SPC water molecules to reproduce full hydration [113] (about 30 water molecules per lipid). The system was slowly heated up to 323 K in the presence of progressively decreasing position restraints on the lipid atoms, over a total period of 0.27 ns. Equilibration was then carried out for 30 ns at 323 K. The need for such an extensive equilibration period is justified by the long timescales associated with the rotation of the lipids around their long axis and with the conformational relaxation of the lipid acyl chains [122]. The final configuration of this trajectory was used directly as initial configuration for the simulation of the bilayer in pure water at 323 K (for the corresponding simulation at 475 K, the temperature was first progressively increased over a time period of 0.24 ns). For the simulations in the presence of disaccharide solutions, the final configuration of the 323 K equilibration trajectory was desolvated (all water molecules deleted). The different systems (low and high concentrations of GNT or TRH) were prepared by randomly placing the appropriate number of sugar molecules in the computational box. The systems were then resolvated to full hydration, imposing a minimal solute–solvent distance of 0.23 nm. A second equilibration procedure (similar to the one described by Pereira et al. [41]) was then applied in order to allow for a proper distribution of the

sugar molecules around the bilayer. More specifically, the systems were heated up to 600 K and equilibrated for 0.56 ns maintaining the coordinates of all lipid atoms constrained. The resulting systems were then energy minimized (with positional constraints on the bilayer atoms) and slowly heated up to the desired temperature (323 or 475 K) in the presence of progressively decreasing position restraints on the lipid atoms, over a period of 0.24 ns. The final configurations of these equilibration trajectories were used directly for the simulations of the bilayer in disaccharide solutions at 323 and 475 K.

The 20 simulations were carried out for a total duration of 10 ns each (after equilibration). A summary of the simulated systems and simulation conditions is provided in Table 1.

Note that a timescale of 10 ns is most likely insufficient to reach full relaxation/sampling for the lipids (e.g. phase transitions in bilayers of simpler lipids already require simulation times on the order of 50–200 ns [123]) and for the sugars (e.g. glycosidic linkage transitions occur on the 50–100 ns timescale [78]). On the other hand, the sugar distribution around the membrane should be appropriately converged, owing to the careful preequilibration protocol (see above). Clearly, simulation timescales on the order of the microsecond would actually be desirable for converged sampling of such sugar-lipid systems. However, the qualitative conclusions of the present work certainly benefit from error cancellation, since they rely on a comparison between a set of 20 closely similar simulations where one parameter is varied at a time (sugar, concentration, temperature or pressure-area conditions). In addition, because the experimental information to compare with is also of qualitative nature (mechanistic hypotheses), the precise numerical results of the simulations are actually less relevant than the observed trends.

2.3. Trajectory analysis

The simulations were analyzed in terms of area per lipid a_{xy} (*NPT* simulations only; $a_{xy} = 0.64\,\mathrm{nm}^2$ in all $NA_{xy}P_zT$ simulations), normalized probability distributions $P_X(z)$ of specific atoms X along the z-axis (bilayer normal), overlaps C_{XY} between the corresponding sugar (GNT or TRH) or water (WAT) atom distribution peaks (X) and lipid headgroup (DPPC) atom distribution peaks (Y), order parameters $S_{CH}(C_n)$ of the methylene (C_n; $n = 2 \ldots 15$) groups in the two lipid acyl chains, and intermolecular H-bonding.

The normalized probability distributions $P_X(z)$ were calculated for selected atoms X of DPPC, GNT, TRH and WAT. The selected atoms were the headgroup phosphorus atom ($X = P$) and the CH_2 glycerol united atom at the sn_1 position ($X = G$) of the lipid molecules (DPPC), the glycosidic oxygen atom ($X = S$) of the sugar molecules (GNT or TRH), and the oxygen atom ($X = W$) of the water molecules (WAT). These distribution profiles were calculated considering last 1 ns of each simulation.

The overlaps between the sugar ($X = S$) or water ($X = W$) distributions on the one hand, and the headgroup phosphate ($Y = P$) or glycerol ($Y = G$) distributions on the other hand, were further quantified in terms of an effective concentration C_{XY} of X in the neighborhood of Y. This quantity is defined as

$$C_{XY} = \frac{N_X}{A_{xy}} \int dz P_X(z) P_Y(z), \tag{1}$$

where N_X is the total number of molecules of species X in the simulation box. The meaning of C_{XY} is most easily understood in the idealized situation where P_Y is constant over some interval Δz and zero outside. In this case, C_{XY} is equal to the total number of molecules of species X present within the region Δz divided by the total volume $A_{xy}\Delta z$ of this region, i.e. to the effective concentration of X in this region. In the general case, C_{XY} can be viewed as a measure of the local concentration of species X at the depth corresponding to species Y within the bilayer. In addition, the ratios C_{SP}/C_{WP} and C_{SG}/C_{WG} can be expressed in terms of local molalities m_P and m_G of the sugar in the regions of the phosphate and glycerol groups, respectively, which can be compared with the corresponding bulk molalities of 0.8 and 1.6 m, and provide an indication concerning the preferential affinity or exclusion of the sugar from the bilayer surface.

Deuterium order parameters (S_{CD}) can be derived from deuterium quadrupole splitting experiments and have being widely used to study biological membranes [124–133] and to validate biomolecular force-fields [114,106]. The corresponding carbon–hydrogen order parameters (S_{CH}) were calculated for the 14 methylene groups in each of the acyl tails of DPPC (sn_1 and sn_2 chains) by computing the correlation functions describing the reorientation of the carbon-hydrogen vectors. More precisely, for each methylene group along the chain, an order parameter tensor $\underline{\mathbf{S}}$ can be defined as $S_{ij} = (1/2)\langle 3cos\theta_i\, cos\theta_j - \delta_{ij}\rangle$, where θ_i is the angle between the i^{th} local molecular axis (x', y' or z') and the bilayer normal (z-axis), δ_{ij} is the Kronecker delta symbol and $\langle \ldots \rangle$ stands for trajectory averaging. Following the convention adopted in previous work [134], for the n th methylene group C_n, the direction of the vector $C_{n-1} - C_{n+1}$ is taken as z', the direction of the vector normal to z' in the plane C_{n-1}, C_n, and C_{n+1} defines y', while x' is the direction of the vector perpendicular both to z' and y'. The quantity $S_{CH} = -(2/3S_{xx} + 1/3S_{yy})$ is the value to be compared with the experimental S_{CD} value [124]. These values were calculated considering the last 4 ns of each simulation, and averaged over the 72 DPPC molecules.

The presence of a H-bond was defined by a maximal hydrogen–oxygen distance of 0.25 nm and a minimal oxygen–hydrogen–oxygen angle of 135°. The occurring intermolecular H-bonds were classified according to the different pairs of species present in the simulations (sugar–sugar, sugar–DPPC, sugar–WAT and DPPC–WAT). All the oxygen atoms of the sugars, WAT and DPPC molecules were considered as H-bond acceptors and all the hydroxyl groups of the sugar and WAT molecules as H-bond donors. In addition, the H-bonded interaction between the sugar and DPPC molecules was further analyzed in terms of H-bonding patterns. A pattern is encoded by a series of integers (listed in decreasing order) indicating the number of H-bonds formed between a sugar molecule and a number of distinct DPPC molecules in a given system configuration. For example, the pattern 311 for a given sugar molecule represents a configuration in which this molecule is simultaneously triply H-bonded to a given DPPC molecule and singly H-bonded to two other DPPC molecules. One characteristic feature of a given pattern is the involved degree of bridging (number of integers in the pattern code), i.e. the number of distinct DPPC molecules forming at least one H-bond with the sugar molecule. The H-bonding analyzes were performed considering the last 4 ns of each simulation.

3. Results

3.1. Area per lipid

The time evolution of the area per lipid a_{xy} as calculated from the 10 simulations performed at constant pressure (*NPT* ensemble) are displayed in Fig. 2. The final values are also reported in Table 1.

The simulations at 323 K evidence a slight decrease in the area per lipid over 10 ns, with final values ranging between 0.57 and 0.60 nm^2. These values are in the expected range for a fully hydrated DPPC bilayer in the liquid-crystalline phase as reported in other simulation studies based on the same force-field [29,41–43], although they are noticeably lower than the consensus experi-

Table 1
Simulated systems and simulation conditions. The different columns report the simulation code (Section 2.2), the thermodynamic ensemble (Section 2.2), the composition of the computational box (number N of molecules of the different species; GNT: gentiobiose; TRH: trehalose; WAT: water; the bilayer patch consists of 2× 6× 6 DPPC molecules in all cases), the disaccharide concentration (c; "m" indicating the solutions molality in mol kg^{-1}), the simulation (thermostat) temperature, the edge lentgh of the (rectangular) computational box along the z-axis (L_z) averaged over the last 1 ns, and the value of the area per lipid (a_{xy}) averaged over the last 1 ns. For these quantities, error estimates are only provided for the *NPT* ensemble. The errors on L_z in the NAP_zT ensemble are very small (0.0005–0.002) due to the constrained a_{xy}. All simulations were carried out for a total duration of 10 ns (after equilibration; Section 2.2). For compactness, entries corresponding to the simulations performed at high temperature are reported between parentheses.

System	Ensemble	N_{GNT}	N_{TRH}	N_{WAT}	c [m]	T [K]	L_z [nm]	a_{xy} [nm^2]
AWL (AWH)	$NA_{xy}P_zT$	–	–	2166	0	323 (475)	6.71 (8.08)	0.640 (0.640)
AG$_l$L (AG$_l$H)	$NA_{xy}P_zT$	36	–	2518	0.79	323 (475)	7.88 (9.23)	0.640 (0.640)
AT$_l$L (AT$_l$H)	$NA_{xy}P_zT$	–	36	2577	0.78	323 (475)	7.90 (9.29)	0.640 (0.640)
AG$_h$L (AG$_h$H)	$NA_{xy}P_zT$	72	–	2581	1.55	323 (475)	8.49 (9.92)	0.640 (0.640)
AT$_h$L (AT$_h$H)	$NA_{xy}P_zT$	–	72	2577	1.55	323 (475)	8.53 (9.82)	0.640 (0.640)
PWL (PWH)	*NPT*	–	–	2166	0	323 (475)	7.53 ± 0.02 (12.75 ± 0.05)	0.568 ± 0.003 (0.401 ± 0.002)
PG$_l$L (PG$_l$H)	*NPT*	36	–	2518	0.79	323 (475)	8.43 ± 0.03 (11.91 ± 0.08)	0.596 ± 0.005 (0.494 ± 0.003)
PT$_l$L (PT$_l$H)	*NPT*	–	36	2577	0.78	323 (475)	8.65 ± 0.03 (12.37 ± 0.08)	0.580 ± 0.004 (0.481 ± 0.004)
PG$_h$L (PG$_h$H)	*NPT*	72	–	2581	1.55	323 (475)	9.09 ± 0.04 (9.27 ± 0.05)	0.598 ± 0.004 (0.681 ± 0.004)
PT$_h$L (PT$_h$H)	*NPT*	–	72	2577	1.55	323 (475)	9.19 ± 0.04 (8.81 ± 0.06)	0.597 ± 0.003 (0.704 ± 0.006)

mental estimate [113] of 0.64 nm^2. As suggested recently [135], the slightly erroneous area per lipid of the GROMOS 45A4 force field for DPPC probably originates from the choice of van der Waals interaction types for specific atom pairs within the headgroups. The above simulations were subsequently extended to 20 ns (data not shown), and did not reveal any significant further decrease in a_{xy} after 10 ns (except for simulation PWL; value of 0.55 nm^2 after 20 ns). However, this discrepancy in a_{xy} (as well as the slight drift in simulation PWL, suggesting the presence of a very slow relaxation process) should not affect the qualitative conclusions of a comparison between the different systems considered. The simulation leading to the lowest value of a_{xy} after 10 ns is the one in the absence of sugars (PWL). The simulations in the presence of sugars lead to a slightly higher value, irrespective of the nature and concentration of the disaccharide.

The time evolution of the area per lipid in the simulations at 475 K is qualitatively very different. In the time interval from 0 to about 2 ns all simulations evidence a substantial increase in the area per lipid. For the systems involving either GNT or TRH at 1.6 m concentration (PG$_h$H and PT$_h$H), a_{xy} remains essentially constant at this higher value (about 0.70–0.75 nm^2). For the other systems (PWH, PG$_l$H and PT$_l$H), a_{xy} decreases rapidly after 2 ns, down to final values ranging between 0.40 and 0.50 nm^2. Here also, the lowest value of a_{xy} after 10 ns is the one in the absence of sugars (PWH). As will be seen below, the three latter systems have essentially lost their bilayer structure at the end of the simulations. Note also that unlike the simulations at 323 K, these simulations cannot be considered to represent an equilibrium situation even after 10 ns.

3.2. Distribution profiles

The normalized probability distributions $P_X(z)$ corresponding to specific DPPC, GNT or TRH, and WAT atoms (X) along the bilayer normal (calculated considering the final 1 ns of the 20 simulations) are displayed in Fig. 3 ($NA_{xy}P_zT$ ensemble) and Fig. 4 (*NPT* ensemble). The corresponding peak overlaps C_{XY} (effective concentration of X in the region Y) are reported in Table 2.

Considering the $NA_{xy}P_zT$ simulations at 323 K, all profiles (Fig. 3) present features characteristic of an intact bilayer structure. The peaks corresponding to the headgroup glycerol and phosphate atoms of the bilayer leaflets are sharp and well separated (separations of about 2.9 and 3.5 nm, respectively), and water penetrates the bilayer no further than the region of the glycerol atoms. When comparing the simulation in pure water (AWL) to the other simulations involving disaccharide solutions (AG$_l$L, AG$_h$L, AT$_l$L, and AT$_h$L), the sugars clearly evidence preferential affinity (compared to water) for the bilayer surfaces, i.e. the sugar molecules cluster at the membrane surface, thereby reducing the water density in this region. However, it is important to stress that: (i) the water replacement is only partial and the membrane headgroups remain significantly hydrated; (ii) the reaching depth of the sugar molecules into the bilayer remains slightly smaller compared to that of water. In the simulations involving 0.8 m sugar solutions (AG$_l$L and AT$_l$L), the surface clustering entirely depletes the bulk from disaccharide molecules. This is no longer the case in the simulations involving 1.6 m sugar solutions (AG$_h$L and AT$_h$L), suggesting that the saturation of the bilayer surface by sugar molecules has been reached between the two bulk concentrations. Experimentally [136], the maximal effect of disaccharides on lipid bilayers

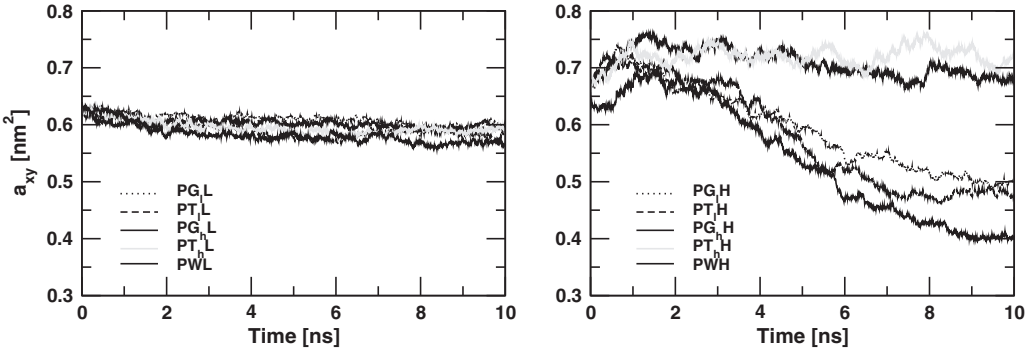

Fig. 2. Time evolution of the area per lipid a_{xy} calculated from the 10 simulations performed at constant pressure (*NPT* ensemble). (Left panel) Simulations at lower temperature (T = 323 K). (Right panel) Simulations at higher temperature (T = 475 K).

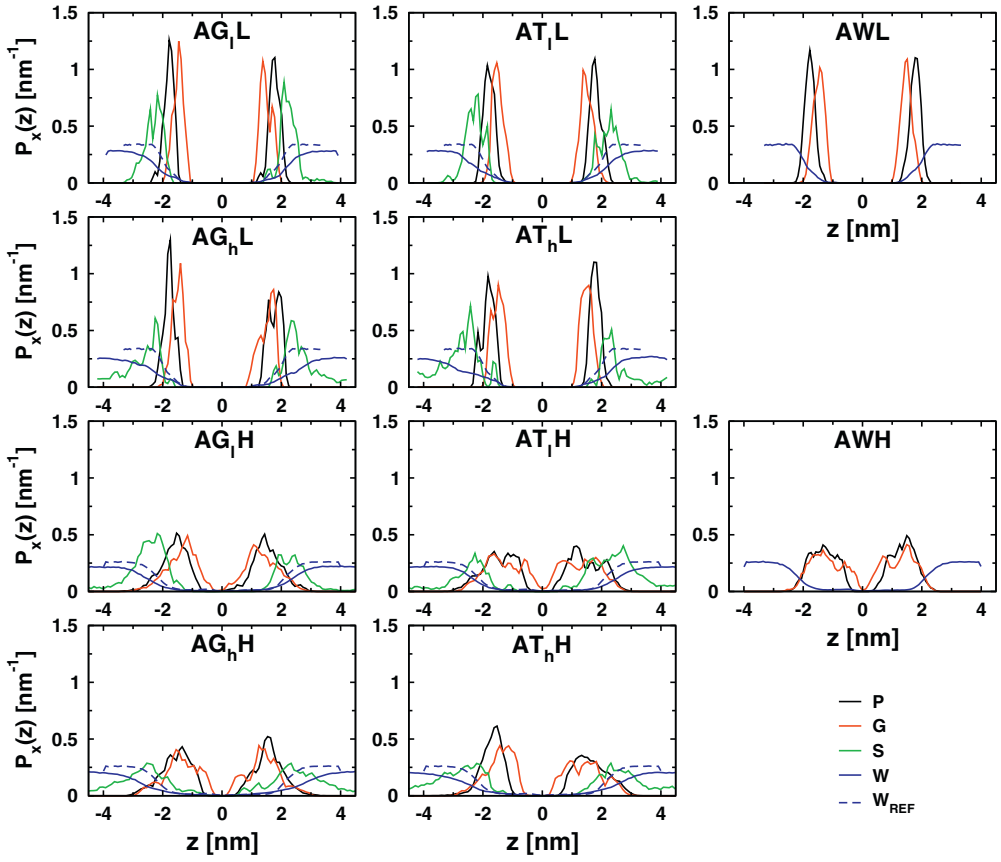

Fig. 3. Normalized probability distributions $P_X(z)$ corresponding to specific DPPC, GNT or TRH, and WAT atoms (X) along the bilayer normal, as calculated from the 10 simulations performed at constant bilayer area ($NA_{xy}P_zT$ ensemble). The different profiles correspond to the phosphorous atom ($X = P$) and the CH_2 glycerol united atom at the sn_1 position ($X = G$) of the lipid molecules (DPPC), to the glycosidic oxygen atom ($X = S$) of the sugar molecules (GNT or TRH), and to the oxygen atom ($X = W$) of the water molecules (WAT). Corresponding distributions of the oxygen atom for the systems in the absence of sugar ($X = W_{ref}$) are also provided. The histogram bin width was set to $L_z/100$ and the profiles are centered at the bilayer midplane (as defined by the center of mass of all lipid atoms along the z-axis). The data was calculated considering the final 1 ns of each simulation. See Table 1 for the definition of the simulation codes.

in terms of inhibiting of the liquid-crystalline to gel phase transition upon dehydration (which is expected to be correlated with the threshold for surface saturation) is reached for a sugar-to-lipid ratio of about 0.75. This is qualitatively consistent with the saturation observed in the present simulations (sugar-to-lipid ratios of 0.5 and 1.0 for the 0.8 and 1.6 m systems, respectively).

Still considering the $NA_{xy}P_zT$ simulations at 323 K, the local concentrations of the disaccharides in the regions of the phosphate (C_{SP}) and glycerol (C_{SG}) groups (Table 2) are on the order of 0.3–0.4 and 0.06–0.13 nm^{-3}, respectively. Upon increasing the bulk sugar concentration from 0.8 to 1.6 m, the former local concentration slightly decreases while the latter slightly increases (for both sugars), suggesting a somewhat deeper penetration of the sugar molecules into the bilayer. However, the small relative magnitude of the change in C_{SP} (decrease by about 5–10% rather than twofold increase) confirms that the membrane surface is already essentially saturated in disaccharide molecules in the presence of a 0.8 m sugar solution. Interestingly, both C_{SP} and C_{SG} are systematically higher for TRH compared to GNT (at both bulk concentrations), indicating a denser coating by the former sugar. The local concentrations of WAT in the regions of the phosphate (C_{WP}) and glycerol (C_{WG}) groups are on the order of 6.5–8.1 and 3.4–4.2 nm^{-3}, respec-

Table 2
Peak overlaps C_{XY} (effective concentration of X in the region Y) derived from the normalized probability distributions of specific atoms (X,Y) along the z-axis (bilayer normal). The different values were calculated according to Eq. (1) based on the distributions $P_X(z)$ and $P_Y(z)$ reported in Figs. 3 and 4, considering the phosphorous atom ($Y = P$) or the CH_2 glycerol united atom ($Y = G$) at the sn_1 position of the lipid molecules (DPPC), along with the glycosidic oxygen atom ($X = S$) of the sugar molecules (GNT or TRH) or the oxygen atom ($X = W$) of the water molecules (WAT). The quantities m_P and m_G correspond to the ratios C_{SP}/C_{WP} and C_{SG}/C_{WG} expressed in terms of molalities. See Table 1 for the definition of the simulation codes.

System	C_{SP} [nm^{-3}]	C_{SG} [nm^{-3}]	C_{WP} [nm^{-3}]	C_{WG} [nm^{-3}]	m_P [mol kg^{-1}]	m_G [mol kg^{-1}]	System	C_{SP} [nm^{-3}]	C_{SG} [nm^{-3}]	C_{WP} [nm^{-3}]	C_{WG} [nm^{-3}]	m_P [mol kg^{-1}]	m_G [mol kg^{-1}]
AWL	–	–	11.65	4.90	–	–	PWL	–	–	10.70	4.43	–	–
AG$_l$L	0.315	0.057	6.53	3.40	2.68	0.93	PG$_l$L	0.212	0.051	7.51	4.59	1.57	0.62
AT$_l$L	0.400	0.096	8.11	4.21	2.74	1.27	PT$_l$L	0.375	0.072	7.98	4.09	2.61	0.98
AG$_h$L	0.299	0.113	6.95	3.87	2.39	1.62	PG$_h$L	0.286	0.037	7.22	3.86	2.20	0.53
AT$_h$L	0.354	0.127	7.52	4.09	2.61	1.72	PT$_h$L	0.320	0.092	7.03	3.56	2.53	1.43
AWH	–	–	2.71	2.66	–	–	PWH	–	–	1.63	1.69	–	–
AG$_l$H	0.211	0.152	3.57	2.86	3.28	2.96	PG$_l$H	0.157	0.137	2.52	2.47	3.46	3.08
AT$_l$H	0.195	0.171	3.68	2.99	2.94	3.18	PT$_l$H	0.250	0.212	2.88	2.79	4.81	4.21
AG$_h$H	0.343	0.290	3.58	3.02	5.32	5.33	PG$_h$H	0.401	0.306	4.06	3.00	5.48	5.66
AT$_h$H	0.347	0.251	4.31	3.45	4.47	4.04	PT$_h$H	0.497	0.248	5.23	3.11	5.28	4.43

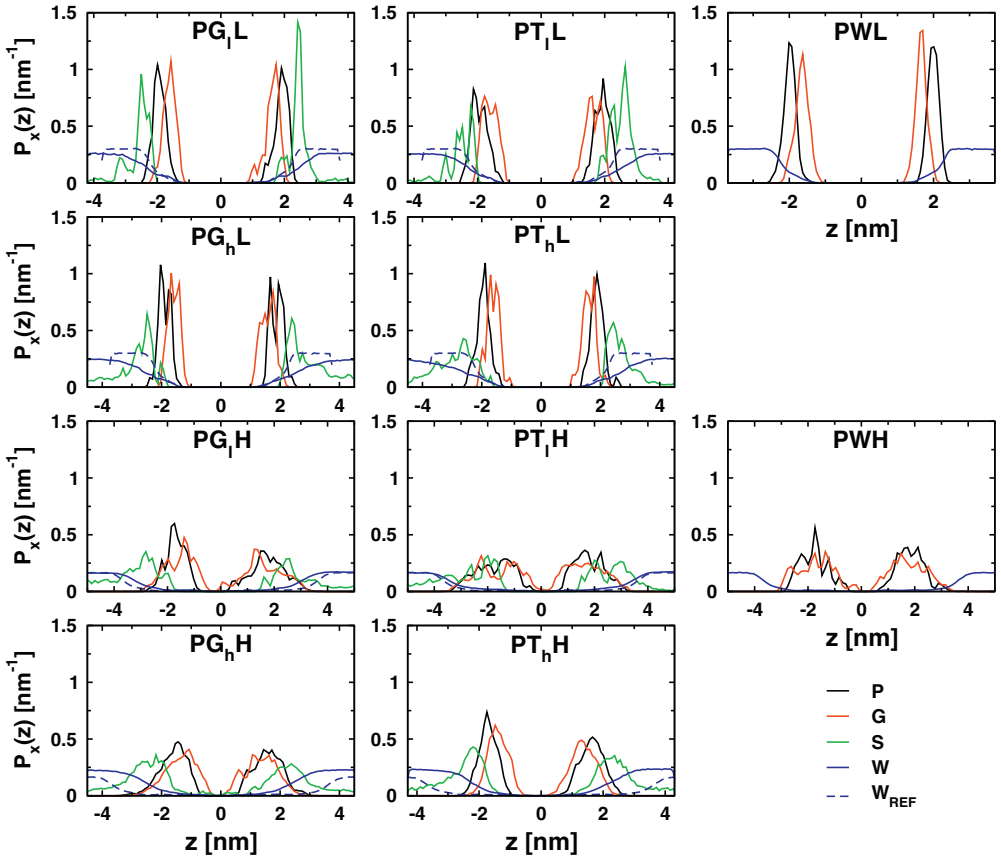

Fig. 4. Normalized probability distributions $P_X(z)$ corresponding to specific DPPC, GNT or TRH, and WAT atoms (X) along the bilayer normal, as calculated from the 10 simulations performed at constant pressure (*NPT* ensemble). The different profiles correspond to the phosphorous atom ($X = P$) and the CH_2 glycerol united atom at the sn_1 position ($X = G$) of the lipid molecules (DPPC), to the glycosidic oxygen atom ($X = S$) of the sugar molecules (GNT or TRH), and to the oxygen atom ($X = W$) of the water molecules (WAT). Corresponding distributions of the oxygen atom for the systems in the absence of sugar ($X = W_{ref}$) are also provided. The histogram bin width was set to $L_z/100$ and the profiles are centered at the bilayer midplane (as defined by the center of mass of all lipid atoms along the z-axis). The data was calculated considering the final 1 ns of each simulation. See Table 1 for the definition of the simulation codes.

tively. The corresponding concentrations in the absence of sugars are significantly higher (11.7 and 4.9 nm^{-3}, respectively), indicating a partial replacement of the water molecules by sugar molecules at the bilayer surface (most pronounced in the phosphate region). Upon increasing the bulk sugar concentration from 0.8 to 1.6 m, the two local concentrations slightly increase for GNT or decrease for TRH (by about 7% in both cases). Here also, both C_{WP} and C_{WG} are systematically higher for TRH compared to GNT (at both bulk concentrations), suggesting a better extent of hydration of the bilayer in the presence of the former sugar, even though this sugar is also the one with the densest surface coating (see above). Finally, the effective sugar molalities in the regions of the phosphate (m_P) and glycerol (m_G) groups are on the order of 2.4–2.7 and 0.9–1.3 (0.8 m bulk concentration) or 1.6–1.7 (1.6 m bulk concentration) mol kg^{-1}, respectively. The effective sugar molality in the phosphate region is significantly higher than in the bulk (preferential affinity) and essentially unaffected by the change in bulk sugar concentration (saturation). The effective sugar molality in the glycerol region is only slightly higher than in the bulk and its dependence on the bulk concentration suggests that saturation has not yet been reached in this region at the 0.8 m bulk concentration. Here also, the values of m_P and m_G are systematically higher for TRH compared to GNT.

Considering the $NA_{xy}P_zT$ simulations at 475 K, all profiles (Fig. 3) present features characteristic of a largely perturbed bilayer structure (with the possible exception of simulation AT$_h$H; see below). The peaks corresponding to the headgroup glycerol and phosphate atoms of the two bilayer leaflets are broad and no longer well separated, indicating that the headgroup and tail regions are no longer clearly distinguishable along the z-axis. Note, however, that a coarse structuring is still visible and that the water molecules still penetrate the lipid volume no further than the region of the glycerol atoms. The effect of elevated temperature is somewhat limited in these simulations because they are performed at constant lateral area and normal pressure ($NA_{xy}P_zT$ ensemble). As a result, an expansion of the box dimension is only possible along the z-axis (Table 1), while the lateral expansion of the bilayer is prohibited. The simulation involving a TRH solution at 1.6 m bulk concentration (AT$_h$H) is clearly distinct from the other simulations in terms of structure preservation. Here, the peaks corresponding to the glycerol and phosphate atoms remain well separated (separations of about 2.3 and 2.8 nm, respectively), so that the headgroup and tail regions can still be recognized. The densities associated with sugar and water molecules also reach much less close to the midplane of the lipid volume.

Still considering the $NA_{xy}P_zT$ simulations at 475 K, the discussion of the local concentrations of the disaccharides (C_{SP} and C_{SG}) or of WAT (C_{WP} and C_{WG}) in the regions of the phosphate and glycerol groups (Table 2) is in most cases not very relevant considering the significant disruption of the bilayer structure. The exception is simulation AT$_h$H, where the bilayer structure is reasonably preserved. Comparing this simulation with the corresponding simulation at low temperature (AT$_h$L), it is seen that C_{SP} is essentially unaltered, C_{SG} increased by about a factor two, C_{WP} decreased by about a factor two and C_{WG} slightly decreased. As a result of these changes, the local molalities m_P and m_G are larger by about 70 and 50%, respectively. In other words, the extent surface coating by TRH has

not changed significantly, but the extent of water replacement has noticeably increased.

Considering the *NPT* simulations at 323 K, the distribution profiles (Fig. 4) and peak overlaps (Table 2) present very similar trends as those observed in the corresponding $NA_{xy}P_zT$ simulations (see above). However, the *NPT* simulations at 475 K present some notable differences. In particular, the distribution profiles corresponding to the systems involving pure water or sugar solutions at 0.8 m concentration (PWH, PG_lH and PT_lH *vs.* AWH, AG_lH and AT_lH) appear to be more affected by the temperature increase in the *NPT* ensemble (see also the dramatic reduction of the area per lipid in these simulations; Section 3.1 and Fig. 2). This is in agreement with previous simulation results [41,42] using the same force-field, showing that the same temperature increase has a much more pronounced disruptive effect (in the absence of sugars) when the bilayer is allowed to expand laterally (*NPT* ensemble). The difference is less pronounced for the system involving GNT at 1.6 m (PG_hH *vs.* AG_hH), although other analyses (see further below) also suggest a more extensive membrane disruption in the *NPT* case. In contrast, the opposite trend is observed for the system involving TRH at 1.6 m (PT_hH *vs.* AT_hH), where the membrane integrity appears to be better preserved under *NPT* compared to $NA_{xy}P_zT$ conditions. Finally, comparing the local concentrations of the disaccharides (C_{SP} and C_{SG}) or of WAT (C_{WP} and C_{WG}) in the regions of the phosphate and glycerol groups (Table 2) for the two latter simulations (PG_hH and PT_hH) with corresponding values in the $NA_{xy}P_zT$ ensemble (AG_hH and AT_hH), it is seen that both C_{SP} and C_{WP} increase (by 17–43%) while C_{SG} and C_{WG} are only moderately altered. These changes are likely due to the lateral expansion of the bilayer (Section 3.1 and Fig. 2), which increases the headgroup accessibility to both water and sugar molecules.

3.3. Order parameters

The order parameters S_{CH} (C_n) corresponding to the 14 methylene groups C_n ($n = 2, \ldots, 15$) in the sn_1 and sn_2 chains of the DPPC molecules (calculated considering the final 4 ns of the 20 simulations) are displayed in Fig. 5 ($NA_{xy}P_zT$ ensemble) and Fig. 6 ($NP_{xy}P_zT$ ensemble). For the sn_2 chain, the calculated values are compared to the experimental carbon–deuterium order parameters (S_{CD}) measured [126] for DPPC in the liquid-crystalline phase at full hydration and at 317.15 K (a single value measured [130] for the methylene group C_2 of the sn_1 chain is also reported).

Considering the $NA_{xy}P_zT$ simulations at 323 K (Fig. 5), the simulation in pure water (AWL) shows reasonable agreement with the experimental values for the sn_2 chain. The calculated values are slightly too low (less order; except for the methylene group C_2) in these simulations at constant lateral area (A_{xy} based on the experimental [113] area per lipid of 0.64 nm^2), while the opposite is usually observed for the present lipid force-field in simulations at constant pressure [29,41,42,106] (*NPT* ensemble; average area per lipid at equilibrium on the order of 0.56 nm^2; see further below). The simulation results suggest comparable values for the order parameters of the two chains, except for the methylene group C_2 (significantly higher value for the sn_1 chain). Although experimental carbon–deuterium order parameters are (to our knowledge) not available for all atoms of the sn_1 chain, a higher value is indeed expected for the latter methylene group [114,130]. When comparing the simulation in pure water (AWL) to the other simulations involving disaccharide solutions (AG_lL, AG_hL, AT_lL, and AT_hL), only limited differences are observed. At the two concentrations considered, both sugars slightly increase the ordering of the sn_1 chain, the effect becoming decreasingly pronounced along the chain (i.e. towards the tail region). In contrast, they tend to rather slightly decrease the ordering of the sn_2 chain. Interestingly, the latter decrease is most pronounced towards the tail region for GNT and towards the headgroup region for TRH (at both sugar concentrations). However, the small magnitude of these changes suggests that the presence of the sugars does not drastically alter the ordering of the lipid chains. Qualitatively similar results were reported previously for sugar–membrane simulations performed at constant pressure [41,42] (*NPT* ensemble).

Considering the $NA_{xy}P_zT$ simulations at 475 K (Fig. 5), the ordering of the chains decreases systematically for all systems compared to the corresponding simulations at 323 K. The effect is most pronounced for the bilayer in the presence of pure water (AWH), followed by the systems at 0.8 m sugar concentration (AG_lH and AT_lH). In contrast, the simulations at 1.6 m sugar concentration (AG_hH and AT_hH) are more ordered, and, in this case, the simulation with TRH shows significantly more ordering compared to that with GNT.

Considering the *NPT* simulations at 323 K (Fig. 6), similar trends are observed as those described above for the $NA_{xy}P_zT$ simulations (see above). The main differences are that: (i) the values calculated for the simulation in pure water (PWL) are now slightly overestimated (more order) compared to the experimental data for the sn_2 chain (this is probably mainly related to the lower average area per lipid within the present force-field; see above); (ii) at the two concentrations considered, GNT slightly decreases the ordering of both sn_1 and sn_2 chains; (iii) at the lowest concentration considered, TRH has essentially no effect on the order parameters of both chains, while a slight decrease is observed at the highest concentration.

Likewise, the trends observed in the *NPT* and $NA_{xy}P_zT$ simulations at 475 K are qualitatively similar. However, the order parameters calculated for the systems with 1.6 m sugar concentration (PG_hH and PT_hH) are significantly higher than in the constant-area case (AG_hH and AT_hH). The difference is particularly spectacular in the case of TRH, where the values are now reaching about half the corresponding values at 323 K. This suggests that the higher protective action of TRH on membranes subjected to stressful conditions may be connected with its stronger response to the lateral expansion of the bilayer (Section 3.2).

A more detailed analysis of time autocorrelation functions associated with the reorientation of various segments of the acyl chains (data not shown) revealed that the changes in order parameters observed in Figs. 5 and 6 are not accompanied by significant changes in the corresponding relaxation times. This suggests that the trends observed in these parameters predominantly reflect structural (decreased ordering of the chains with respect to the bilayer normal) rather than dynamic (increased mobility) effects.

3.4. Bilayer structure

The final configurations of the 10 ns simulations are displayed in Fig. 7 ($NA_{xy}P_zT$ ensemble) and Fig. 8 (*NPT* ensemble).

Considering the $NA_{xy}P_zT$ simulations at 323 K (Fig. 7) and irrespective of the solution environment, the bilayer presents a similar structure and is clearly found in the liquid-crystalline phase, in which the hydrophobic tails are flexible and partially disordered. At 0.8 m sugar concentration (AG_lL and AT_lL), most of the carbohydrate molecules interact with the bilayer headgroups and only few of them are totally exposed to the bulk solvent. At 1.6 m sugar concentration (AG_hL and AT_hL), the bilayer surfaces are more densely coated, and several sugar molecules are found to interact only with other sugar molecules or/and with the solvent (but not with the lipid headgroups).

Considering the $NA_{xy}P_zT$ simulations at 475 K (Fig. 7) and irrespective of the solution environment, the bilayer structure is found to be largely perturbed as a result of the increased thermal motion (with the possible exception of simulation AT_hH; see below). The largest perturbation is observed for the simulation in pure water (AWL), which evidences a complete disruption of the bilayer struc-

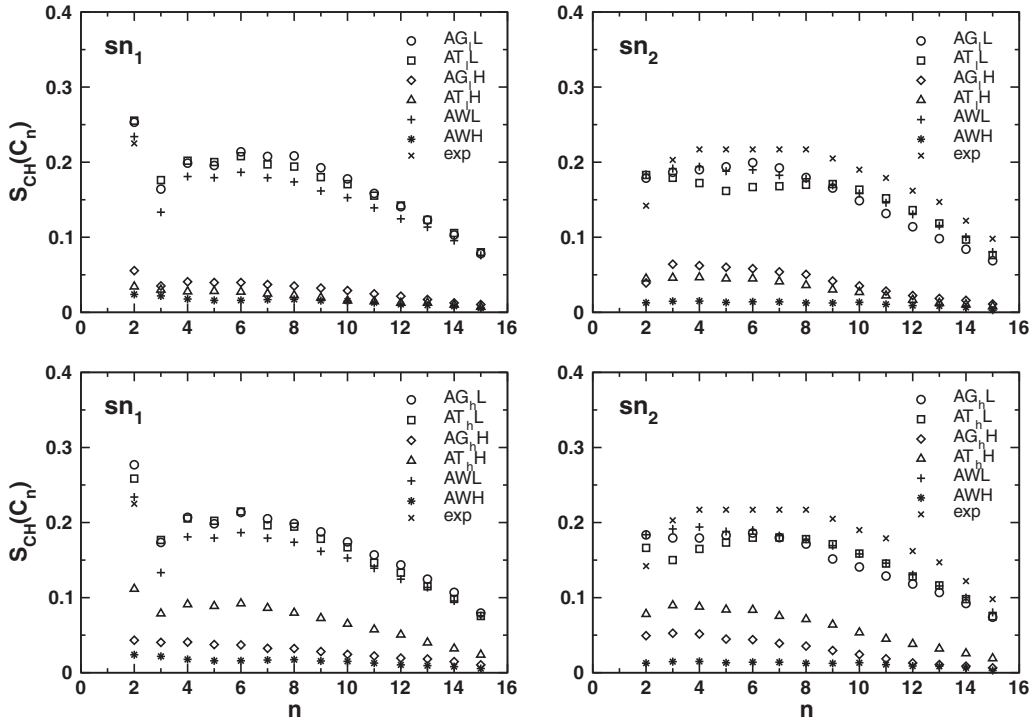

Fig. 5. Order parameters corresponding to the 14 methylene groups in the sn_1 (left) and sn_2 (right) chains of the DPPC molecules, as calculated from the 10 simulations performed at constant bilayer area ($NA_{xy}P_zT$ ensemble). The sn_2 chain is the one connected to the glycerol CH_1 group (i.e. the chain vicinal to the phosphate group), while the sn_1 chain is the one located on the second CH_2 group (i.e. most distant from the phosphate group). The experimental carbon–deuterium order parameters S_{CD} for the sn_2 chain measured [113] in the liquid-crystalline phase at full hydration and at 317.15 K are reported for comparison. A single experimental value available for the methylene group C_2 of the sn_1 chain [130] is also reported. The data was calculated (Section 2.3) based on the final 4 ns of each simulation. See Table 1 for the simulations codes.

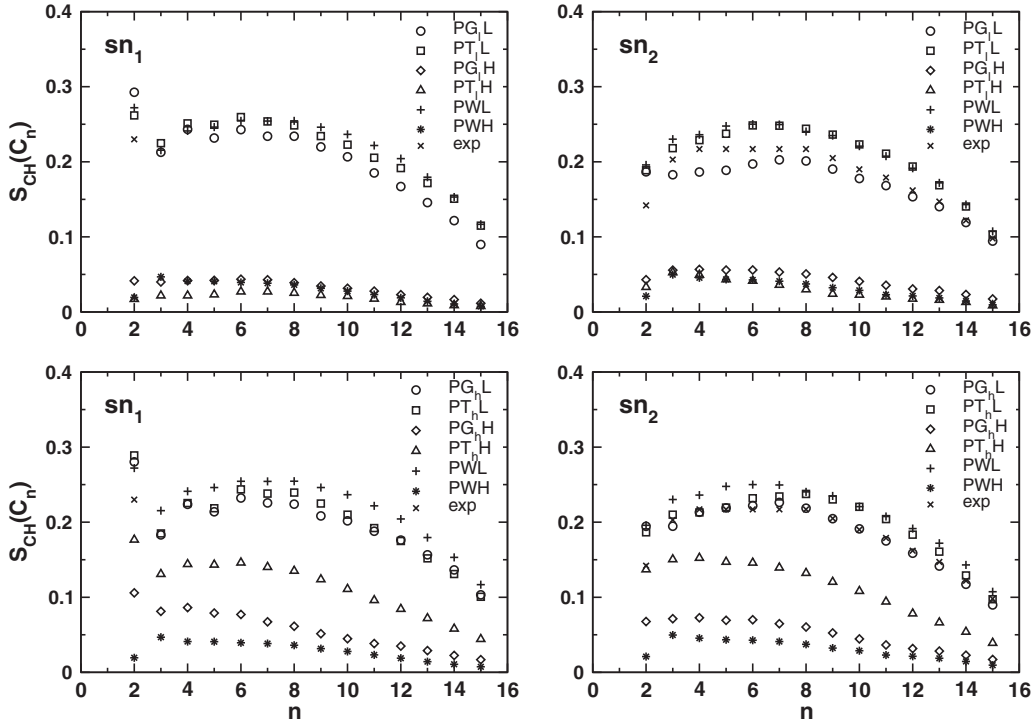

Fig. 6. Order parameters corresponding to the 14 methylene groups in the sn_1 (left) and sn_2 (right) chains of the DPPC molecules, as calculated from the 10 simulations performed at constant pressure (*NPT* ensemble). The sn_2 chain is the one connected to the glycerol CH_1 group (i.e. the chain vicinal to the phosphate group), while the sn_1 chain is the one located on the second CH_2 group (i.e. most distant from the phosphate group). The experimental carbon–deuterium order parameters S_{CD} for the sn_2 chain measured [113] in the liquid-crystalline phase at full hydration and at 317.15 K are reported for comparison. A single experimental value available for the methylene group C_2 of the sn_1 chain [130] is also reported. The data was calculated (Section 2.3) based on the final 4 ns of each simulation. See Table 1 for the simulations codes.

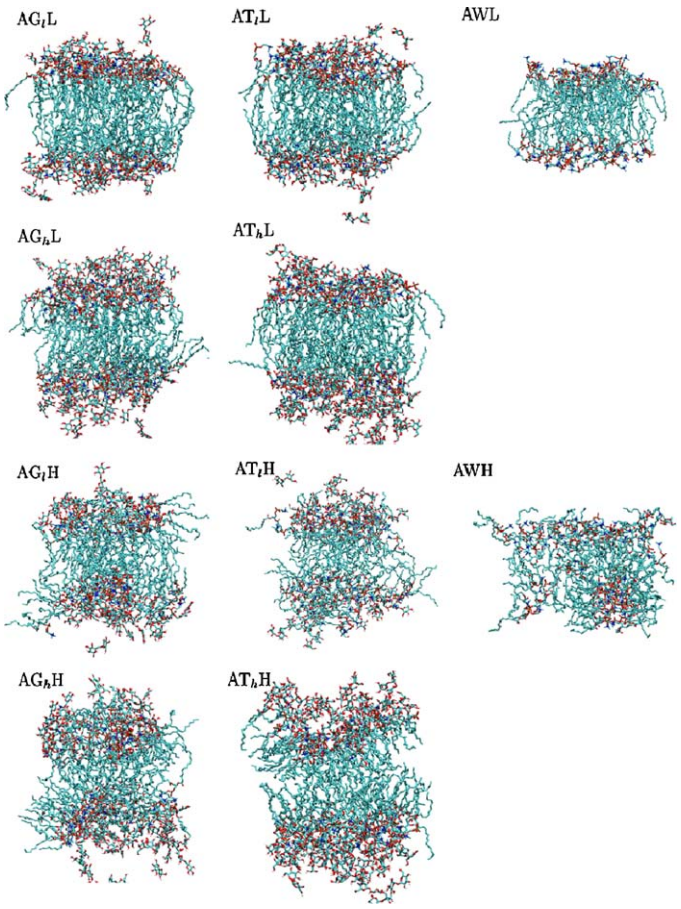

Fig. 7. Final configurations of the simulations performed at constant bilayer area ($NA_{xy}P_zT$ ensemble). The configurations correspond to the end of the 10 ns simulations. DPPC and sugar molecules are represented using a stick model. Water molecules have been removed for clarity. Carbon atoms are represented in gray, oxygen atoms in red, phosphorus atoms in yellow, nitrogen atoms in blue and hydrogen atoms in white. See Table 1 for the definition of the simulation codes. (For interpretation of the references to color in this figure legend, the reader is referred to the web version of the article.)

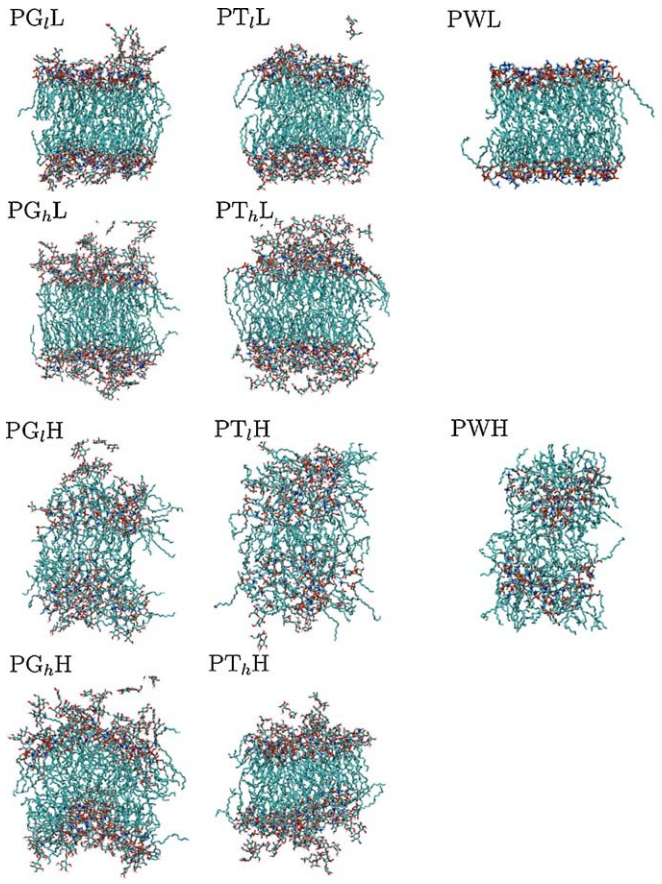

Fig. 8. Final configurations of the simulations performed at constant pressure (*NPT* ensemble). The configurations correspond to the end of the 10 ns simulations. DPPC and sugar molecules are represented using a stick model. Water molecules have been removed for clarity. Carbon atoms are represented in gray, oxygen atoms in red, phosphorus atoms in yellow, nitrogen atoms in blue and hydrogen atoms in white. See Table 1 for the definition of the simulation codes.

ture. At 0.8 m sugar concentration (AG$_l$H and AT$_l$H), the bilayer structure is also mostly disrupted. At 1.6 m sugar concentration (AG$_h$H and AT$_h$H), the results for GNT are similar. However, the simulation in the presence of the TRH solution evidences a much lower extent of disorder, and the structure clearly remains closest to that of a bilayer in the liquid-crystalline phase. Comparison with, e.g. the final structure of the corresponding simulation at 323 K (AT$_h$L) shows that the headgroups still arrange in two well defined surfaces (although deviating more significantly from planarity), that the lipid tails are preferentially ordered along the bilayer normal (although with a lower extent of ordering) and that the lipid tails from the two leaflets do not interdigitate significantly (even close to the bilayer midplane). For TRH, qualitatively similar results were reported previously for sugar–membrane simulations performed at constant pressure [41,42], at the same temperatures and at 1 or 2 m sugar concentration (*NPT* ensemble). In particular, in these independent simulations (using the same force-field), TRH also only promoted a significant extent of structure preservation at high temperature for the highest bulk concentration considered.

Considering the *NPT* simulations at 323 K (Fig. 8) the final structures are qualitatively comparable to those observed at the end of the corresponding $NA_{xy}P_zT$ simulations (see above). However, more pronounced differences are visible at 475 K. For the simulations in pure water or at 0.8 m sugar concentration (PWH, PG$_l$H and PT$_l$H) the bilayer structure is entirely lost (i.e. even more disrupted than in the corresponding $NA_{xy}P_zT$ simulations). In contrast, for the simulations at 1.6 m sugar concentration (PG$_h$H and PT$_h$H), the bilayers are slightly expanded laterally and the bilayer structure is largely preserved. The structure preservation is more evident in the presence of TRH compared to GNT.

3.5. Hydrogen-bonding

The occurrences of hydrogen bonds (average over the last 4 ns of the simulations) between all the species present in the different systems are reported in Table 3 for the 20 simulations.

Considering the $NA_{xy}P_zT$ simulations at 323 K, both sugars are found to form a significant number of H-bonds to the lipid headgroups, with an average of about 2.0–2.1 (0.8 m solutions) or 1.1–1.2 (1.6 m solutions) H-bonds per sugar molecule. The observation that this number decreases by about a factor of two upon doubling the bulk sugar concentration is again indicative that the saturation of the bilayer surface in sugar molecules has essentially been reached between the two bulk concentrations considered. The number of sugar-headgroup H-bonds is slightly lower for TRH compared to GNT (at both bulk concentrations), although the difference is small (about 2–3, i.e. 3–4%). On the other hand, the number of headgroup-water H-bonds is significantly higher in the TRH solutions compared to the GNT solutions (at identical bulk concentration), the difference being larger (about 10–30, i.e. 5–15%). Consistent with previous studies [29,41–43,62], the total number

Table 3
Occurrences of intermolecular H-bonds between the different species in the systems, as calculated from the 20 different simulations. The occurrences n_{XY} are reported in the form of average numbers of H-bonds of the given type in the system, distinguishing DPPC lipid (L), sugar (S) and water (W) molecules. The data was calculated (Section 2.3) considering the final 4 ns of each simulation. The estimated errors were averaged over the entire data set and are in the range of 2–4%. See Table 1 for the definition of the simulation codes.

System	n_{LS}	n_{LW}	$n_{LS}+n_{LW}$	n_{SS}	n_{SW}	System	n_{LS}	n_{LW}	$n_{LS}+n_{LW}$	n_{SS}	n_{SW}
AWL	–	336.6	336.6	–	–	PWL	–	309.1	309.1	–	–
AG_lL	74.7	231.2	305.9	35.4	373.7	PG_lL	72.2	250.3	322.5	32.0	387.1
AT_lL	71.6	263.5	335.1	56.9	353.7	PT_lL	59.9	260.2	320.1	50.9	380.5
AG_hL	83.4	228.8	312.2	146.3	774.4	PG_hL	82.6	219.5	302.1	146.9	782.2
AT_hL	81.1	240.6	321.7	159.4	760.4	PT_hL	84.9	221.2	306.1	160.8	753.5
AWH	–	163.8	163.8	–	–	PWH	–	129.3	129.3	–	–
AG_lH	58.2	144.1	202.3	31.4	257.2	PG_lH	51.5	133.6	185.1	30.9	258.1
AT_lH	53.6	147.2	200.8	49.4	245.6	PT_lH	64.8	145.3	210.1	54.8	224.8
AG_hH	102.3	125.7	228.0	94.3	478.8	PG_hH	110.8	144.2	255.0	89.9	488.6
AT_hH	81.0	148.2	229.2	119.9	515.3	PT_hH	91.2	156.4	247.6	123.6	510.8

of H-bonds between the lipid headgroups and their solution environment (sugar and water molecules) is only weakly affected by the possible presence (and concentration) of the cosolutes (suggesting a mere exchange of H-bonding partners for the lipid headgroups, the total number of H-bonding sites provided by the membrane remaining about constant). This observation is accurately valid in the case of TRH (AWL *vs.* AT_lL *vs.* AT_hL), but a decrease (by about 25–30, i.e. 7–9%) in this total number of H-bonds (relative to the situation of the bilayer in pure water) is apparent for GNT (AWL *vs.* AG_lL *vs.* AG_hL). Finally, a systematic difference between GNT and TRH is also observed in the number of sugar–sugar and sugar–water H-bonds (at identical sugar concentration). The former number is significantly lower for GNT (by about 15–20, i.e. 8–38%), while the latter is significantly lower for TRH (by about 15–20, i.e. 2–5%).

Considering the $NA_{xy}P_zT$ simulations at 475 K, the interpretation of average H-bond numbers can only reveal qualitative trends considering that the bilayer is disrupted. Overall, the number of sugar-headgroup H-bonds is reduced compared to the corresponding simulations at 323 K. The possible exceptions are AG_hH (slightly increased) and AT_hH (essentially unaltered). In all cases, the number of headgroup-water H-bonds is dramatically reduced (by a factor 1.6–1.8) upon increasing the temperature. The number of sugar-headgroup H-bonds is still lower for TRH compared to GNT, while the number of headgroup-water H-bonds is still higher in the TRH solutions compared to the GNT solutions. The numbers of sugar–sugar as well as sugar–water H-bonds all systematically decrease upon increasing the temperature. Here also, the trends observed at 323 K persist at 475 K. GNT forms fewer sugar–sugar H-bonds compared to TRH, while TRH forms fewer sugar–water H-bonds compared to GNT.

Considering the *NPT* simulations at 323 K, the differences with respect to the corresponding $NA_{xy}P_zT$ simulations are again limited and the same qualitative trends are observed (saturation effect between 0.8 and 1.6 m sugar concentration, near conservation of the total number of H-bonds between the lipid headgroups and their solution environment, higher number of sugar–sugar and lower number of sugar–water H-bonds for TRH compared to GNT). However, the simulations in pure water (PWL) shows a smaller number of headgroup-water H-bonds (by about 28, i.e. 8%) compared to the corresponding simulations at constant area (AWL). This result is probably related to the smaller value of area per lipid (Section 3.1 and Fig. 2). Note also that the number of sugar-headgroup H-bonds is more markedly lower for TRH compared to GNT at 0.8 m concentration (by about 12, i.e. 17%), while it is now slightly higher at 1.6 m concentration (by about 2, i.e. 2%).

Considering the *NPT* simulations at 475 K, and focusing on the simulations at 1.6 m sugar concentration (PG_hH and PT_hH) where the bilayer structure is well preserved, a higher number of sugar-headgroup H-bonds (by about 8–10, i.e. 8–13%) and headgroup-water (by about 10–19, i.e. 7–15%) is observed compared to the corresponding $NA_{xy}P_zT$ simulations (AG_hH and AT_hH). Here also, this increase is probably related to the slightly larger area per lipid in the former simulations (Section 3.1 and Fig. 2). Comparing these two simulations at 475 K to the corresponding simulations at 323 K, the temperature increase is seen to result for both disaccharides in a noticeable increase in the number of sugar-headgroup H-bonds (along with a decrease in the number of headgroup-water H-bonds), in agreement with the results of previous sugar–membrane simulations [41,42] performed at constant pressure (*NPT* ensemble).

The (absolute and relative) contributions of H-bonds involving the phosphate or the ester groups to the total number of sugar–lipid H-bonds are reported in the Table 4.

Considering the $NA_{xy}P_zT$ and *NPT* simulations at 323 K and irrespective of the sugar concentration, both sugars form a lower number of H-bonds with the ester groups (about 30–40%) compared to the phosphate groups of the lipids. In the $NA_{xy}P_zT$ ensemble, in addition to the slightly higher total number of sugar-lipid H-bonds (Table 3), the systems with GNT also evidence a higher proportion of H-bonds to the ester groups compared to those with TRH, suggesting a somewhat deeper penetration of GNT inside the membrane. However, this difference is no longer observed in the *NPT* ensemble, where both disaccharides present a comparable proportion of H-bonds to the ester groups (about 30%) at both concentrations.

Considering the $NA_{xy}P_zT$ and *NPT* simulations at 475 K, the proportion of H-bonds to the ester groups (40–50%) is significantly increased compared to 323 K. For the simulations at 1.6 m sugar concentration, the corresponding increase observed for GNT (Table 3) nearly exclusively involves H-bonds to the ester groups, while for TRH, the absence of net change (Table 3) still hides an increase in the proportion of H-bonds to the ester groups.

The distribution of the sugar molecules among different H-bonding patterns and associated degrees of bridging are reported in Table 5.

Considering the $NA_{xy}P_zT$ and *NPT* simulations at 323 K, most of the sugar molecules that are H-bonded to the lipids belong to the patterns 1, 11, 111, 2, 21 and 211, i.e. are (possibly multiple times) H-bonded to 1, 2 or 3 lipid molecules, although many other patterns (involving the bridging of up to 6 lipid molecules) do occur in the simulations. Upon increasing the sugar concentration, most of the additional sugar molecules do not bind to the lipids (saturation), although the numbers of sugar molecules H-bonded to 1 or 2 distinct lipid headgroups (as well as 3 in the *NPT* simulations) still noticeably increase. The comparison of GNT and TRH solutions (at both bulk concentrations) does not reveal clear systematic differences in terms of H-bonding patterns.

Considering the $NA_{xy}P_zT$ and *NPT* simulations at 475 K, the same H-bonding patterns are significantly populated. In the $NA_{xy}P_zT$ ensemble, comparison with the simulations at 323 K suggests

Table 4
Occurrences and relative contributions of H-bonds involving the phosphate ($n_{LS}(P)$) or the ester ($n_{LS}(E)$) groups to the total number of H-bonds formed between sugar and lipid molecules (n_{LS} in Table 3). The data was calculated (Section 2.3) considering the final 4 ns of each simulation. The estimated errors were averaged over the entire data set and are in the range of 2–4%. See Table 1 for the definition of the simulation codes.

System	n_{LS}	$n_{LS}(P)$	$n_{LS}(E)$	$n_{LS}(P)/n_{LS}$ [%]	$n_{LS}(E)/n_{LS}$ [%]	System	n_{LS}	$n_{LS}(P)$	$n_{LS}(E)$	$n_{LS}(P)/n_{LS}$ [%]	$n_{LS}(E)/n_{LS}$ [%]
AG_lL	74.7	45.1	29.6	60.4	39.6	PG_lL	72.2	49.8	22.3	69.1	30.9
AT_lL	71.6	49.3	22.3	68.9	31.1	PT_lL	59.9	41.8	18.2	69.7	30.3
AG_hL	83.4	55.5	28.0	66.5	33.5	PG_hL	82.6	56.2	26.4	68.1	31.9
AT_hL	81.1	58.3	22.8	71.9	28.1	PT_hL	84.9	57.8	27.1	68.1	31.9
AG_lH	58.2	30.9	27.3	53.1	46.9	PG_hH	51.5	28.6	22.9	55.6	44.4
AT_lH	53.6	29.5	24.1	55.0	45.0	PT_lH	64.8	35.3	29.5	54.5	45.5
AG_hH	102.3	48.4	53.9	47.3	52.7	PG_hH	110.8	58.8	52.0	53.1	46.9
AT_hH	81.0	49.5	31.5	61.0	39.0	PT_hH	91.2	54.6	36.5	59.9	40.1

Table 5
Average numbers of sugar molecules forming a specific H-bonding pattern (top) or characterized by a specific degree of bridging (bottom) with lipid molecules, as calculated from the 20 simulations. A pattern is encoded by a series of integers (listed in decreasing order) indicating the number of H-bonds formed between a sugar molecule and a number of distinct DPPC molecules in a given system configuration. The degree of bridging (number of integers in the pattern code), represents the number of distinct DPPC molecules forming at least one H-bond with the sugar molecule. The data was calculated (Section 2.3) considering the final 4 ns of each simulation. The estimated errors were averaged over the entire data set and are in the range of 2–4%. See Table 1 for the definition of the simulation codes.

Pattern	AG_lL	AT_lL	AG_hL	AT_hL	AG_lH	AT_lH	AG_hH	AT_hH	PG_lL	PT_lL	PG_hL	PT_hL	PG_lH	PT_lH	PG_hH	PT_hH
0	7.1	6.4	34.4	34.6	11.8	12.8	31.7	35.50	8.4	9.0	37.1	34.9	16.3	12.8	27.9	30.3
1	7.0	8.8	13.3	13.5	6.2	7.4	10.5	13.0	7.3	8.6	10.4	11.7	4.4	5.9	12.1	14.5
11	6.0	5.6	7.7	8.6	3.4	4.2	4.6	6.7	5.4	6.7	6.6	6.2	2.6	3.7	5.8	8.5
111	2.7	3.6	2.4	2.3	1.2	1.7	1.9	2.5	2.4	2.9	2.4	2.8	1.3	1.9	2.1	2.7
1111	0.2	0.4	0.1	0.2	0.4	0.5	0.6	0.5	1.0	0.5	0.1	0.3	0.5	0.9	0.5	0.5
11111	0.1	–	0.0	0.1	0.1	0.1	0.1	0.1	0.3	–	0.0	0.0	0.1	0.3	0.1	0.0
2	2.6	2.5	4.4	3.3	4.9	2.8	7.4	4.1	2.6	2.0	4.3	3.2	3.3	2.0	7.2	4.5
21	4.6	2.6	4.8	4.5	3.9	2.6	6.0	4.0	3.5	2.9	4.1	7.9	3.0	2.3	6.4	5.1
211	2.7	2.2	1.8	2.7	1.9	1.7	4.1	2.4	2.0	2.5	2.9	3.1	2.0	1.9	4.2	2.6
2111	0.6	0.8	0.3	0.7	0.7	0.6	1.9	0.8	1.0	0.3	0.6	0.8	0.8	1.4	1.9	0.6
21111	0.3	0.1	0.1	0.2	0.1	0.1	0.4	0.1	0.3	0.0	0.0	0.0	0.1	0.5	0.5	0.1
211111	0.2	–	0.0	–	0.0	–	0.0	0.0	0.2	–	0.0	–	0.0	0.1	0.1	0.0
22	0.1	0.0	0.3	0.2	0.3	0.1	0.3	0.2	0.1	0.0	1.1	0.1	0.3	0.1	0.3	0.2
221	0.1	0.1	1.0	0.4	0.2	0.2	0.3	0.3	0.1	0.3	0.9	0.2	0.2	0.3	0.5	0.3
2211	0.1	0.2	0.1	0.1	0.1	0.1	0.3	0.1	0.1	0.0	0.2	0.0	0.1	0.4	0.3	0.1
22111	0.4	0.0	0.4	0.0	0.0	0.0	0.1	0.0	0.3	0.0	0.0	–	0.0	0.1	0.1	0.0
221111	0.2	–	–	–	0.0	–	0.0	–	0.4	–	0.0	–	0.0	0.0	0.0	0.0
3	0.2	0.5	0.4	0.1	0.4	0.4	0.6	0.6	0.3	0.2	0.2	0.2	0.3	0.3	0.7	0.7
31	0.4	1.4	0.2	0.2	0.3	0.4	0.5	0.5	0.2	0.1	0.5	0.4	0.4	0.3	0.6	0.7
311	0.3	0.4	0.1	0.4	0.1	0.2	0.3	0.3	0.1	0.1	0.4	0.2	0.2	0.3	0.4	0.3
3111	0.1	0.1	–	0.1	0.0	0.1	0.1	0.1	0.0	0.0	0.1	0.0	0.0	0.2	0.2	0.1
31111	0.0	0.1	–	0.0	0.0	–	0.0	0.0	0.0	0.0	0.0	0.0	0.0	0.0	0.1	0.0
32	0.0	–	0.0	–	0.0	0.0	0.0	0.0	–	0.0	–	0.0	0.0	0.0	0.1	0.1
321	–	–	–	–	0.0	0.0	0.0	0.0	–	0.0	0.0	0.0	0.0	0.1	0.0	0.0
3211	–	–	–	–	0.0	0.0	0.0	0.0	0.0	0.0	–	0.0	0.0	0.1	0.0	0.0
4	0.0	0.0	0.0	–	0.0	0.0	0.0	0.1	0.0	0.0	0.0	0.0	0.0	0.0	0.0	0.1
41	0.0	0.0	–	–	0.0	0.0	0.0	0.1	–	0.0	0.0	0.0	0.0	0.0	0.0	0.1
Total	36	36	72	72	36	36	72	72	36	36	72	72	36	36	72	72
Degree of bridging																
0	7.1	6.4	34.3	34.6	11.8	12.8	31.7	35.5	8.4	9.0	37.1	34.9	16.3	12.8	27.9	30.3
1	9.8	11.8	18.0	16.9	11.5	10.7	18.6	17.7	10.2	10.8	14.9	15.1	8.0	8.2	10.0	19.8
2	11.0	9.7	13.1	13.5	7.8	7.3	11.3	11.6	9.2	9.7	12.3	14.6	6.3	6.4	13.2	14.7
3	5.9	6.3	5.3	5.8	3.5	3.9	6.7	5.5	4.6	5.8	6.6	6.3	3.7	4.5	7.2	5.8
4	1.0	1.5	0.5	1.1	1.2	1.2	1.2	1.5	2.1	0.8	1.0	1.1	1.4	3.0	2.8	1.3
Other	1.3	0.3	0.9	0.3	0.3	0.2	0.7	0.3	1.5	–	0.1	–	0.3	1.1	0.9	0.1
Total	36	36	72	72	36	36	72	72	36	36	72	72	36	36	72	72

a trend towards a decrease in the number of sugar molecules H-bonded to 2 or 3 distinct lipid molecules for GNT at 1.6 m concentration (AG_hL *vs.* AG_hH). In the latter case, the increase in the number of sugar–lipid H-bonds is predominantly associated with the patterns 2, 21, 211 and 2111. In the *NPT* simulations at 1.6 m sugar concentration (PG_hH and PT_hH), the higher number of sugar-headgroup H-bonds (compared to the corresponding $NA_{xy}P_zT$ simulations) is predominantly associated with sugar molecules H-bonded to 2, 3 and 4 lipid molecules. Comparing these two *NPT* simulations at 475 K to the corresponding simulations at 323 K, the temperature increase is seen to result (for both disaccharides) in the enhancement of all patterns involving the bridging of multiple lipid molecules, in agreement with the results of previous sugar–membrane simulations performed at constant pressure [41,42] (*NPT* ensemble).

4. Conclusion

When comparing the influence of the two disaccharides on the bilayer, it is important to emphasize the very close similarity between the two compounds (Fig. 1). The two sugars are constitutional isomers (i.e. they share an identical atom content). They possess the same total number of hydroxyl or hydroxymethyl groups (8), all oriented equatorially around the two pyranose rings (with the slight difference that TRH has two hydroxymethyl groups compared to one only for GNT) and the same number of ring (2)

and glycosidic (1) oxygen atoms. Furthermore, the non-bonded interaction parameters (atomic partial charges and van der Waals interaction parameters) within the 45A4 force-field [103] are very similarly distributed in the two compounds (so that partial cancellation of possible force-field errors can be expected). As a result, the only significant difference resides in the presence of an extra dihedral angle within the glycosidic linkage of GNT compared to TRH. As discussed in Section 1, however, this difference has a considerable impact on the flexibility. The differences observed in the present simulations concerning the influence of TRH and GNT on a lipid bilayer can thus be predominantly attributed to a difference in intrinsic flexibility.

According to the sugar-like mechanism proposed by Pereira and Hünenberger [29], both sugars should evidence preferential affinity (compared to water) for the membrane surface. However, TRH, due to its lower conformational entropy (reduced entropic penalty of rigidification), is expected to present a stronger preferential affinity compared to GNT. In agreement with this proposed mechanism, the present results at 323 K support a preferential affinity of the two sugars for the bilayer surfaces, a significant extent of sugar–lipid H-bonding, an essentially identical number of H-bonds between the lipid headgroups and their solution environment irrespective of the nature and concentration of the sugar, and a stronger preferential affinity for TRH compared to GNT (as judged by the local sugar molalities in the headgroup region). However, these simulations also reveal four other important differences between the two sugars: (i) a higher extent of residual bilayer hydration for TRH compared to GNT (Tables 2 and 3); (ii) a higher extent of sugar–sugar H-bonding (sugar clustering) for TRH compared to GNT (Table 3); (iii) a more limited extent of sugar–lipid H-bonding for TRH compared to GNT (Table 3); (iv) a more limited depth of penetration into the bilayer (H-bonds to the ester *vs.* phosphate groups; in the $NA_{xy}P_zT$ simulations) for TRH compared to GNT (Table 4). These observations may also be indirectly related to the particular conformational properties of the TRH molecule (high propensity to self-association, strong hydrophilicity, lack of flexibility). Finally, both sugars present a significant extent of H-bonded bridging of the lipid molecules.

The conformational entropies of the two types of sugar molecules in the presence of the lipid bilayer can actually be estimated directly based on the simulated trajectories using quasi-harmonic analysis [137]. The corresponding average values (over the 72 disaccharide molecules) for simulations PG_hL and PT_hL were calculated and compared to those obtained previously for single molecules of the two sugars in aqueous solution [78]. The resulting estimates for $-T\Delta S_{solution\rightarrow bilayer}$ are of about +20 and $-3\,kJ\,mol^{-1}$ for GNT and TRH, respectively. In spite of the qualitative nature of these estimates, the very large difference supports the hypothesis of a high entropic cost (rigidification) upon binding GNT molecules to a bilayer, and a corresponding negligible cost for the corresponding binding of (already inherently rigid) TRH molecules.

The simulations at 475 K show that at sufficiently high bulk concentration, TRH is indeed superior to GNT in preserving the integrity of the bilayer structure. The efficiency of TRH in preserving the bilayer structure under those conditions is observed in two distinct simulations ($NA_{xy}P_zT$ and NPT), and corroborated by previous independent simulations [41]. It seems therefore logical to correlate the observed (and experimentally supported) higher bioprotective ability of TRH with one or more of the above-mentioned features. However, it appears that these features encompass elements of at least four of the hypotheses formulated in Section 1 for the bioprotective action of sugars. The partial replacement of lipid-water by sugar-lipid H-bonds is compatible with the WRH. However, the idea that such a replacement is a key element of the bioprotection mechanism seems contradicted by the observation that the extent of sugar-lipid H-bonding is nearly systematically higher for GNT compared to TRH in the present simulations (at all bulk concentrations and temperatures considered). The presence of a significant extent of H-bonded bridging of the lipid headgroups by sugar molecules is compatible with the HBH. However, the idea that such a replacement is a key element of the bioprotection mechanism is also somewhat at odds with the observation that the extent of bridging is about identical for GNT compared to TRH at 323 K, and generally higher at 475 K. The more significant extent of residual hydration of the bilayer surface for TRH compared to GNT is also clearly reminiscent of the WEH. Finally, the higher extent of sugar clustering for TRH compared to GNT suggests an increased viscosity, closely related to the VIH. On the other hand, the results of the present simulations (as well as of a number of previous simulation studies) definitely support preferential affinity (rather than preferential exclusion) of the sugar molecules for the bilayer surface, in disagreement with the HFH.

The compatibility of the present (and previous experimental [5,9,7,19–26,30–40,44–60] and computational [41–43,63–72]) observations with the WRH, HBH, VIH and WEH appears somewhat surprising at first sight. A first possible interpretation is that multiple mechanisms are simultaneously active. A second one is that multiple mechanisms are potentially active, their relevance depending on the nature and intensity of the environmental stress, as well as on the type of protected biostructure. A third one is that some of the observed features are mere consequences of the others, and do not bear relevance as driving forces for bioprotection. And a fourth one is simply that the proposed mechanisms are not defined precisely enough for an unambiguous assessment based on experimental or theoretical data. We believe that the fourth point is actually very relevant: although the five mechanisms represent valid qualitative (pictorial) interpretations, they lack a clear quantitative (measurable) definition. In particular, it seems essential to include into the formulation of each: (i) a clear mention of the type of biomolecule considered; (ii) a clear specification of the experimental conditions (temperature, pressure, concentration regime); (iii) a quantitative definition for intuitive concepts such as “preferential affinity”, “water replacement”, “headgroup bridging” or “water entrapment”. The suggestion of revised definitions for these hypotheses, along with an overview of the experimental and theoretical data supporting each of them would represent an essential step in the characterization of bioprotection mechanisms and will be the scope of forthcoming work.

Acknowledgments

Financial support from the Swiss National Science Foundation (Grant 21-121895) is gratefully acknowledged. The authors would also like to thank Cristina Pereira, Maria Reif and Anna-Pitschna Kunz for fruitful discussions.

References

[1] E.P. Feovilova, Deceleration of vital activity as a universal biochemical mechanism ensuring adaptation of microorganisms to stress factors: a review, Appl. Biochem. Microbiol. 39 (2003) 1–18.
[2] A.I. Zhmakin, Physical aspects of cryobiology, Physics-Uspekhi 51 (2008) 231–252.
[3] D. Keilin, The Leeuwenhoek lecture: the problem of anabiosis or latent life: history and current concept, Proc. R. Soc. Lond. B: Biol. Sci. 150 (1959) 149–191.
[4] J.S. Clegg, Cryptobiosis—a peculiar state of biological organization, Comp. Biochem. Physiol. 128B (2001) 613–624.
[5] J.H. Crowe, F.A. Hoekstra, L.M. Crowe, Anhydrobiosis, Annu. Rev. Physiol. 54 (1992) 579–599.
[6] M. Guppy, P. Withers, Metabolic depression in animals: physiological perspectives and biochemical generalization, Biol. Rev. 74 (1999) 1–40.
[7] J.H. Crowe, L.M. Crowe, W.F. Wolkers, A.E. Oliver, X. Ma, J.-H. Auh, M. Tang, S. Zhu, J. Norris, F. Tablin, Stabilization of dry mammalian cells: lessons from nature, Integr. Comp. Biol. 45 (2005) 810–820.

[8] S. Hengherr, A.G. Heyer, H. Koehler, Trehalose and anhydrobiosis in tardigrades—evidence for divergence in responses to dehydration, FEBS J. 275 (2008) 281–288.
[9] L.M. Crowe, Lessons from nature: the role of sugars in anhydrobiosis, Comp. Biochem. Physiol. 131A (2002) 505–513.
[10] J.H. Crowe, A.E. Oliver, F. Tablin, Is there a single biochemical adaptation to anhydrobiosis, Integr. Comp. Biol. 42 (2002) 497–503.
[11] J.H. Crowe, Trehalose as a "chemical chaperone": fact and fantas, in: P. Csermely, L. Vigh (Eds.), In: Molecular Aspects of the Stress Response: Chaperones, Membranes and Network, vol. 13, Landes Bioscience and Springer Science + Business Media, 2007, pp. 497–503.
[12] V. Ragoonan, A. Aksan, Heterogenity in desiccated solutions: implications for biostabilization, Biophys. J. 94 (2008) 2212–2227.
[13] L. D'Alfonso, M. Collini, F. Cannone, G. Chirico, B. Campanini, G. Cottone, L. Cordone, GFP-mut2 proteins in trehalose–water matrixes: spatially heterogeneous protein–water–sugar structure, Biophys. J. 93 (2007) 284–293.
[14] F. Attanasio, Trehalose effects on α-crystallin aggregates, Biochem. Biophys. Res. Commun. 354 (2007) 899–905.
[15] R.P. Baptista, Thermodynamics and mechanism of cutinase stabilization by trehalose, Biopolymers 89 (2008) 538–547.
[16] R.B. Best, N.-V. Buchete, G. Hummer, Supporting information: are current molecular dynamics force fields too helical? Biophys. J. 95 (2008) L07–L09.
[17] G. Bellavia, L. Cordone, A. Cupane, Calorimetric study of myoglobin embedded in trehalose–water matrixes, J. Therm. Anal. Calorim. 95 (2009) 699–702.
[18] N.K. Jain, I. Roy, Effect of trehalose on protein structure, Protein Sci. 18 (2009) 24–36.
[19] J.H. Crowe, L.M. Crowe, J.F. Carpenter, C.A. Wistrom, Stabilization of dry phospholipid bilayers and proteins by sugar, Biochem. J. 242 (1987) 1–10.
[20] J.H. Crowe, L.M. Crowe, A.E. Oliver, N. Tsvetkova, W. Wolkers, F. Tablin, The trehalose myth revisited: introduction to a symposium on stablilization of cells in the dry state, Cryobiology 43 (2001) 89–105.
[21] C. Cacela, D.K. Hincha, Monosaccharide composition, chain length and linkage type influence the interactions of oligosaccharides with dry phosphatidylcholine membrane, Biophys. Biochim. Acta 1758 (2006) 680–691.
[22] C. Cacela, D.K. Hincha, Low amounts of sucrose are sufficient to depress the phase transition temperature of dry phosphatidylcholine, but not for lyoprotection of liposomes, Biophys. J. 90 (2006) 2831–2842.
[23] J.L. Holovati, J.P. Acker, Spectrophotometric measurement of intraliposomal trehalose, Cryobiology 55 (2007) 98–107.
[24] S. Ohtake, C. Schebor, S.P. Palecek, J.J. de Pablo, Effect of sugar–phosphate mixtures on the stability of DPPC membranes in dehydrated systems, Cryobiology 48 (2004) 81–89.
[25] S. Ohtake, C. Schebor, J.J. de Pablo, Effect of trehalose on the phase behaviour of DPPC–cholesterol unilamellar vesicles, Biochem. Biophys. Acta 1758 (2006) 65–73.
[26] A.E. Oliver, E.L. Kendall, M.C. Howland, B. Sanii, A.P. Shreve, A.N. Parikh, Protecting, patterning, and scaffolding supported lipid membranes using carbohydrate glasses, Lab Chip 8 (2008) 892–897.
[27] B. Zhu, T. Furuki, T. Okuda, Sakurai, Natural DNA mixed with trehalose persists in B-form double stranding even in the dry state, J. Phys. Chem. 111 (2007) 5542–5544.
[28] C. Santivarangkna, B. Higl, P. Foerst, Protection mechanisms of sugars during different stages of preparation process of dried lactic acid starter culture, Food Microbiol. 25 (2008) 429–441.
[29] C.S. Pereira, P.H. Hünenberger, The influence of polyhydroxylated compounds on a hydrated phospholipid bilayer: a molecular dynamics study, Mol. Simul. 34 (2008) 403–420.
[30] J.H. Crowe, L.M. Crowe, D. Chapman, Preservation of membranes in anhydrobiotic organisms: the role of trehalose, Science 223 (1984) 701–703.
[31] C.W.B. Lee, J.S. Waugh, R.G. Griffin, Solid-state NMR study of trehalose/1,2-dipalmitoyl-sn-phosphatidylcholine interaction, Biochemistry 25 (1986) 3737–3742.
[32] M. Nakagaki, H. Nagase, H. Ueda, Stabilization of the lamellar structure of phosphatidylcholine by complex formation with trehalose, J. Membr. Sci. 73 (1992) 173–180.
[33] N.M. Tsvetkova, B.L. Phillips, L.M. Crowe, J.H. Crowe, S.H. Risbud, Effect of sugars on headgroup mobility in freeze-dried dipalmitoylphosphatidylcholine bilayers: solid-state 31P NMR and FTIR studies, Biophys. J. 75 (1998) 2947–2955.
[34] J.H. Crowe, J.F. Carpenter, L.M. Crowe, The role of vitrification in anhydrobiosis, Annu. Rev. Physiol. 60 (1998) 73–103.
[35] M.C. Luzardo, F. Amalfa, A.M. Nunez, S. Diaz, A.C. Biondi de Lopez, E.A. Disalvo, Effect of trehalose and sucrose on the hydration and dipole potential of lipid bilayers, Biophys. J. 78 (2000) 2452–2458.
[36] C. Lambruschini, A. Relini, A. Ridi, L. Cordone, A. Gliozzi, Trehalose interacts with phospholipid polar heads in Langmuir monolayer, Langmuir 16 (2000) 5467–5470.
[37] F.A. Hoekstra, E.A. Golovina, J. Buitink, Mechanisms of plant desiccation tolerance, J. Trends Plant Sci. 6 (2001) 431–438.
[38] D.K. Hincha, E. Zuther, E.M. Hellwege, A.G. Heyer, Specific effects of fructo- and gluco-oligosaccharides in the preservation of liposomes during drying, Glycobiology 12 (2002) 103–110.
[39] J. Ricker, N. Tsvetkova, W. Wolkers, C. Leidy, F. Tablin, M. Longo, J. Crowe, Trehalose maintains phase separation in an air-dried binary lipid mixture, Biophys. J. 84 (2003) 3045–3051.
[40] D.K. Hincha, M. Hagemann, Stabilization of model membranes during drying by compatible solutes involved in the stress tolerance of plants and microorganisms, Biochem. J. 383 (2004) 277–283.
[41] C.S. Pereira, R.D. Lins, I. Chandrasekhar, L.C.G. Freitas, P.H. Hünenberger, Interaction of the disaccharide trehalose with a phospholipid bilayer: a molecular dynamics study, Biophys. J. 86 (2004) 2273–2285.
[42] C.S. Pereira, P.H. Hünenberger, Interaction of the sugars trehalose, maltose and glucose with a phospholipid bilayer: a comparative molecular dynamics study, J. Phys. Chem. B 110 (2006) 15572–15581.
[43] C.S. Pereira, P.H. Hünenberger, Effect of trehalose on a phospholipid membrane under mechanical stress, Biophys. J. 95 (2008) 3525–3534.
[44] R.J. Williams, A.C. Leopold, The glassy state in corn embryos, Plant. Physiol. 89 (1989) 977–981.
[45] J.L. Green, C.A. Angell, Phase relations and vitrification in saccharide–water solutions and the trehalose anomaly, J. Phys. Chem. 93 (1989) 2880–2882.
[46] W.Q. Sun, A.C. Leopold, Glassy state and seed storage stability: a viability equation analysis, Ann. Bot. 74 (1994) 601–604.
[47] K.L. Koster, M.S. Webb, G. Bryant, D.V. Lynch, Interactions between soluble sugars and POPC (1-palmitoyl-2-oleoylphosphatidylcholine) during dehydration: vitrification of sugars alters the phase behavior of the phospholipid, Biochim. Biophys. Acta 1193 (1994) 143–150.
[48] W.Q. Sun, A.C. Leopold, L.M. Crowe, J.H. Crowe, Stability of dry liposomes in sugar glasses, Biophys. J. 70 (1996) 1769–1776.
[49] W.Q. Sun, A.C. Leopold, Cytoplasmic vitrification and survival of anhydrobiotic organisms—a viability equation analysis, Comp. Biochem. Physiol. A (1997) 327–333.
[50] K.L. Koster, Y.P. Lei, M. Anderson, S. Martin, G. Bryant, Effects of vitrified and nonvitrified sugars on phosphatidylcholine fluid-to-gel phase transition, Biophys. J. 78 (2000) 1932–1946.
[51] P.S. Belton, A.M. Gil, IR and Raman spectroscopic studies on the interaction of trehalose with hen egg white lysozyme, Biopolymers 34 (1994) 957–961.
[52] I.G. Tironi, B.A. Luty, W.F. van Gunsteren, Space–time correlated reaction field: a stochastic dynamical approach to the dielectric continuum, J. Chem. Phys. 106 (1997) 6068–6075.
[53] G. Cottone, G. Ciccotti, L. Cordone, Protein–trehalose–water structures in trehalose coated carboxy-myoglobin, J. Chem. Phys. 117 (2002) 9862–9866.
[54] R.D. Lins, S.C. Pereira, P.H. Hünenberger, Trehalose–protein interaction in aqueous solution, Proteins: Struct. Funct. Bioinform. 55 (2004) 177–186.
[55] S. Giuffrida, G. Cottone, L. Cordone, Structure-dynamics coupling between protein and external matrix in sucrose-coated and in trehalose-coated MbCO: an FTIR study, J. Phys. Chem. B 108 (2004) 15415–15421.
[56] A.M. Massari, I.J. Finkelstein, B.L. McClain, A. Goj, X. Wen, K.L. Bren, R.F. Loring, M.D. Fayer, The influence of aqueous versus glassy solvents on protein dynamics: vibrational echo experiments and molecular dynamics simulations, J. Am. Chem. Soc. 127 (2005) 14279–14289.
[57] L. Cordone, G. Cottone, S. Giuffrida, G. Palazzo, G. Venturoli, C. Viappiani, Internal dynamics and protein-matrix coupling in trehalose-coated protein, Biochim. Biophys. Acta 1749 (2005) 252–281.
[58] T. Lenne, C.J. Garvey, K.L. Koster, G. Bryant, Effects of sugars on lipid bilayer during dehydration—SAXS/WAXS measurement and quantitative mode, J. Phys. Chem. B 113 (2009) 2486–2491.
[59] P. Westh, Glucose, sucrose and trehalose are partially excluded from the interface of hydrated DMPC bilayers, Phys. Chem. Chem. Phys. 10 (2008) 4110–4112.
[60] R.P. Rand, V.A. Parsegian, Hydration forces between phospholipid bilayer, Biochim. Biophys. Acta 988 (1989) 351–376.
[61] M. Sakurai, T. Furuki, K. Akao, D. Tanaka, Y. Nakahara, T. Kikawada, M. Watanabe, T. Okuda, Vitrification is essential for anhydrobiosis in an African chironomid polypedilum vanderplanki, PNAS 105 (2008) 5093–5098.
[62] D.P. Geerke, W.F. van Gunsteren, P.H. Hünenberger, Molecular dynamics simulations of the interaction between polyhydroxylated compounds and Lennard–Jones walls: preferential affinity/exclusion effects and their relevance for bioprotection, Mol. Simul. 36 (2010) 708–728.
[63] A.K. Sum, R. Faller, J.J. de Pablo, Molecular simulation study of phospholipid bilayers and insights of the interactions with disaccharide, Biophys. J. 85 (2003) 2830–2844.
[64] A.K. Sum, Molecular simulation study of the influence of small molecules on the dynamic and structural properties of phospholipid bilayer, Chem. Biodivers. 2 (2005) 1503–1516.
[65] M. Doxastakis, A.K. Sum, J.J. de Pablo, Modulating membrane properties: the effect of trehalose and cholesterol on a phospholipid bilayer, J. Phys. Chem. B 109 (2005) 24173–24181.
[66] A. Skibinsky, R.M. Venable, R.W. Pastor, A molecular dynamics study of the response of lipid bilayers and monolayers to trehalose, Biophys. J. 89 (2005) 4111–4121.
[67] S. Leekumjorn, A.K. Sum, Molecular simulation study of structural and dynamic properties of mixed DPPC/DPPE bilayer, Biophys. J. 90 (2006) 3951–3965.
[68] S. Leekumjorn, A.K. Sum, Molecular investigation of the interactions of trehalose with lipid bilayers of DPPC, DPPE and their mixture, Mol. Simul. 32 (2006) 219–230.
[69] T. Róg, I. Vattulainen, A. Bunker, M. Karttunen, Glycolipid membranes through atomistic simulations: effect of glucose and galactose head groups on lipid bilayer properties, J. Phys. Chem. B 111 (2007) 10146–10154.

[70] G. van den Bogaart, N. Hermans, V. Krasnikov, A.H. de Vries, B. Poolman, On the decrease in lateral mobility of phospholipids by sugars, Biophys. J. 92 (2007) 1598–1605.
[71] S. Leekumjorn, Y. Wu, A.K. Sum, C. Chan, Experimental and computational studies investigating trehalose protection of hepG2 cells from palmitate-induced toxicity, Biophys. J. 94 (2008) 2869–2883.
[72] S. Leekumjorn, A.K. Sum, Molecular dynamics study on the stabilization of dehydrated lipid bilayers with glucose and trehalose, J. Phys. Chem. B 112 (2008) 10732–10740.
[73] G. Xie, S.N. Timasheff, The thermodynamic mechanism of protein stabilization by trehalose, Biophys. Chem. 64 (1997) 25–43.
[74] J.E. Curtis, T.E. Dirama, G.A. Carri, D.J. Tobias, Inertial suppresion of protein dynamics in a binary glycerol–trehalose glass, J. Phys. Chem. Lett. 110 (2006) 22953–22956.
[75] F.-F. Liu, X.-Y. Dong, Y. Sun, Molecular mechanism for the effects of trehalose on β-hairpin folding revealed by molecular dynamics simulation, J. Mol. Graph. Model. 27 (2008) 421–429.
[76] G. Cottone, A comparative study of carboxy myoglobin in saccharide–water systems by molecular dynamics simulation, J. Phys. Chem. B 111 (2007) 3563–3569.
[77] N. Smolin, R. Winter, Effect of temperature, pressure and cosolvents on structural and dynamic properties of the hydration shell of SNase: a molecular dynamics computer simulation study, J. Phys. Chem. B 112 (2008) 997–1006.
[78] L. Perić-Hassler, H.S. Hansen, R. Baron, P.H. Hünenberger, Conformational properties of glucose-based disaccharides using molecular dynamics simulations with local elevation umbrella sampling, Carbohydr. Res. 345 (2010) 1781–1801.
[79] C.S. Pereira, D. Kony, R. Baron, M. Müller, W.F. van Gunsteren, P.H. Hünenberger, Conformational and dynamical properties of disaccharides in water: a molecular dynamics study, Biophys. J. 90 (2006) 4337–4344.
[80] C.S. Pereira, D. Kony, R. Baron, M. Müller, W.F. van Gunsteren, P.H. Hünenberger, Erratum to "Conformational and dynamical properties of disaccharides in water: a molecular dynamics study" [J. Phys. Chem. B 110, 15572–15581 (2006)], Biophys. J. 93 (2007) 706–707.
[81] A.B. Richards, S. Krakowka, L.B. Dexter, H. Schmid, A.P.M. Wolterbeek, D.H. Waalkens-Berendsen, A. Shigoyuki, M. Kurimoto, Trehalose: a review of properties, history of use and human tolerance, and results of multiple safety studies, Food Chem. Toxicol. 40 (2002) 871–898.
[82] F. Albertorio, V.A. Chapa, X. Chen, A.J. Diaz, P.S. Cremer, The α,α-(1→1) linkage of trehalose is key to anhydrobiotic preservation, J. Am. Chem. Soc. 129 (2007) 10567–10574.
[83] M.C. Donnamaria, E.I. Howard, J.G. Grigera, Interaction of water with α,α-trehalose in solution: molecular dynamics simulation approach, J. Chem. Soc., Faraday Trans. 90 (1994) 2731–2735.
[84] S. Magazu, G. Maisano, H.D. Middendorf, P. Migliardo, A.M. Musolino, V. Villari, α, α-trehalose–water solutions. II. Influence of hydrogen bond connectivity on transport properties, J. Phys. Chem. B 102 (1998) 2060–2063.
[85] E. Iannilli, E. Tettamanti, L. Galantini, S. Magazú, An integrated quasi-elastic light-scattering, pulse-gradient-spin-echo study on the transport properties of α,α-trehalose, sucrose, and maltose deuterium oxide solutions, J. Phys. Chem. B (2001) 12143–12149.
[86] M.K. Dowd, A.D. French, P.J. Reilly, Modeling of aldopyranosyl ring puckering with MM3(92), Carbohydr. Res. 264 (1994) 1–19.
[87] Q. Liu, R.K. Schmidt, B. Teo, P.A. Karplus, J.W. Brady, Molecular dynamics studies of the hydration of α,α-trehalose, J. Am. Chem. Soc. 119 (1997) 7851–7862.
[88] G. Bonanno, R. Noto, S.L. Fornili, Water interaction with α,α-trehalose: molecular dynamics simulation, J. Chem. Soc., Faraday Trans. 94 (1998) 2755–2762.
[89] P.B. Conrad, J.J. de Pablo, Computer simulation of the cryoprotectant disaccharide α,α-trehalose in aqueous solution, J. Phys. Chem. A 103 (1999) 4049–4055.
[90] S.B. Engelsen, S. Pérez, Unique similarity of the asymmetric trehalose solid-state hydration and the diluted aqueous-solution hydration, J. Phys. Chem. B 104 (2000) 9301–9311.
[91] P. Bordat, A. Lerbret, J.-P. Demaret, F. Affouard, M. Descamps, Comparative study of trehalose, sucrose and maltose in water solutions by molecular modelling, Europhys. Lett. 65 (2004) 41–47.
[92] A. Lerbret, P. Bordat, F. Affouard, M. Descamps, F. Migliardo, How homogeneous are trehalose, maltose, and surcose water solutions? An insight from molecular synamics simulations, J. Phys. Chem. B 109 (2005) 11046–11057.
[93] A. Lerbret, P. Bordat, F. Affouard, Y. Guinet, A. Hédoux, L. Paccou, D. Prévost, M. Descamps, Influence of homologous disaccharides on the hydrogen-bond network of water: complementary Raman scattering experiments and molecular dynamics simulations, Carbohydr. Res. 340 (2005) 881–887.
[94] Y. Choi, K.W. Cho, K. Jeong, S. Jung, Molecular dynamics simulations of trehalose as a dynamic reducer for solvent water molecules in the hydration shell, Carbohydr. Res. 341 (2006) 1020–1028.
[95] T. Chen, A. Fowler, M. Toner, Literature review: supplemented phase diagram of the trehalose–water binary mixture, Cryobiology 40 (2000) 277–282.
[96] Y. Luo, W. Li, W. Wang, Trehalose: protector of antixodant enzymes or reactive oxygen species scavenger under heat stress, Environ. Exp. Bot. 63 (2008) 378–384.
[97] F. Béranger, C. Crozet, A. Goldsborough, S. Lehmann, Trehalose impairs aggregation of PrP^{Sc} molecules and protects prion-infected cells against oxidative damage, Biochem. Biophys. Res. Commun. 374 (2008) 44–48.
[98] A. Buléon, V. Tran, Systematic conformational search for the branching point of amylopectin, Int. J. Biol. Macromol. 12 (1990) 345–352.
[99] A. Imberty, S. Pérez, Conformational analysis and molecular modelling of the branching point of amylopectin, Int. J. Biol. Macromol. 11 (1989) 177–185.
[100] D. Kony, W. Damm, S. Stoll, W.F. van Gunsteren, P.H. Hünenberger, Explicit-solvent molecular dynamics simulations of the polysaccharide schizophyllan in water, Biophys. J. 93 (2007) 442–455.
[101] W.F. van Gunsteren, S.R. Billeter, A.A. Eising, P.H. Hünenberger, P. Krüger, A.E. Mark, W.R.P. Scott, I.G. Tironi, Biomolecular Simulation: The GROMOS96 Manual and User Guide, Verlag der Fachvereine, Zürich, Switzerland, 1996.
[102] W.R.P. Scott, P.H. Hünenberger, I.G. Tironi, A.E. Mark, S.R. Billeter, J. Fennen, A.E. Torda, T. Huber, P. Krüger, W.F. van Gunsteren, The GROMOS biomolecular simulation program package, J. Phys. Chem. A 103 (1999) 3596–3607.
[103] R.D. Lins, P.H. Hünenberger, A new GROMOS force field for hexopyranose-based carbohydrates, J. Comput. Chem. 26 (2005) 1400–1412.
[104] L.D. Schuler, W.F. van Gunsteren, On the choice of dihedral angle potential energy functions for *n*-alkanes, Mol. Simul. 25 (2000) 301–319.
[105] L.D. Schuler, X. Daura, W.F. van Gunsteren, An improved GROMOS96 force field for aliphatic hydrocarbons in the condensed phase, J. Comput. Chem. 22 (2001) 1205–1218.
[106] I. Chandrasekhar, M.A. Kastenholz, R.D. Lins, C. Oostenbrink, L.D. Schüler, D.P. Tieleman, W.F. van Gunsteren, A consistent potential energy parameter set for lipids: dipalmitoylphosphatidylcholine as a benchmark of the GROMOS96 45A3 force field, Eur. Biophys. J. 32 (2003) 67–77.
[107] T.A. Soares, P.H. Hünenberger, M.A. Kastenholz, V. Kräutler, T. Lenz, R.D. Lins, C. Oostenbrink, W.F. van Gunsteren, An improved nucleic-acid parameter set for the GROMOS force field, J. Comput. Chem. 26 (2005) 725–737.
[108] V. Kräutler, M. Müller, P.H. Hünenberger, Conformation, dynamics, solvation and relative stabilities of selected β-hexopyranoses in water: a molecular dynamics study with the GROMOS 45A4 force field, Carbohydr. Res. 342 (2007) 2097–2124.
[109] H.S. Hansen, P.H. Hünenberger, Using the local elevation method to construct optimized umbrella sampling potentials: calculation of the relative free energies and interconversion barriers of glucopyranose ring conformers in water, J. Comput. Chem. 31 (2010) 1–23.
[110] H.J.C. Berendsen, J.P.M. Postma, W.F. van Gunsteren, J. Hermans, Interaction models for water in relation to protein hydration, in: B. Pullman (Ed.), Intermolecular Forces, Reidel, Dordrecht, The Netherlands, 1981, pp. 1–23.
[111] R.W. Hockney, The potential calculation and some applications, Methods Comput. Phys. 9 (1970) 136–211.
[112] J.-P. Ryckaert, G. Ciccotti, H.J.C. Berendsen, Numerical integration of the Cartesian equations of motion of a system with constraints: molecular dynamics of n-alkanes, J. Comput. Phys. 23 (1977) 327–341.
[113] J.F. Nagle, S. Tristram-Nagle, Structure of lipid bilayers, Biochim. Biophys. Acta 1469 (2000) 159–195.
[114] J.B. Klauda, R.M. Venable, A.D. MacKerell, R.W. Pastor Jr., Considerations for lipid force field development, Curr. Top. Membr. 60 (2008) 1–48.
[115] H.J.C. Berendsen, J.P.M. Postma, W.F. van Gunsteren, A. Di Nola, J.R. Haak, Molecular dynamics with coupling to an external bath, J. Chem. Phys. 81 (1984) 3684–3690.
[116] W.F. van Gunsteren, H.J.C. Berendsen, Computer simulation of molecular dynamics: methodology, applications and perspectives in chemistry, Angew. Chem. Int. Ed. 29 (1990) 992–1023.
[117] J.A. Barker, R.O. Watts, Monte Carlo studies of the dielectric properties of water-like models, Mol. Phys. 26 (1973) 789–792.
[118] I.G. Tironi, R. Sperb, P.E. Smith, W.F. van Gunsteren, A generalized reaction field method for molecular dynamics simulations, J. Chem. Phys. 102 (1995) 5451–5459.
[119] T.N. Heinz, W.F. van Gunsteren, P.H. Hünenberger, Comparison of four methods to compute the dielectric permittivity of liquids from molecular dynamics simulations, J. Chem. Phys. 115 (2001) 1125–1136.
[120] Y. Zhu, J. Zajicek, A.S. Serianni, Acyclic forms of [1-^{13}C]aldohexoses in aqueous solution: quantitation by ^{13}C NMR and deuterium isotope effects on tautomeric equilibria, J. Org. Chem. 66 (2001) 6244–6251.
[121] M.U. Roslund, P. Tähtinen, M. Niemitz, R. Sjöholm, Complete assignments of the ^{1}H and ^{13}C chemical shifts and $J_{H,H}$ coupling constants in NMR spectra of D-glucopyranose and all D-glucopyranosyl-D-glucopyranosides, Carbohydr. Res. 343 (2008) 101–112.
[122] Y. Takaoka, M. Pasenkievicz-Gierula, H. Miyagawa, K. Kitamura, Y. Tamura, A. Kusumi, Molecular dynamics generation of nonarbitrary membrane models reveals lipid orientational correlations, Biophys. J. 79 (2000) 3118–3138.
[123] B.A.C. Horta, A.H. de Vries, P.H. Hünenberger, Simulating the transition between gel and liquid-crystal phases of lipidbilayers: dependence of the transition temperature on the hydration level, J. Chem. Theory Comput. 6 (2010) 2488–2500.
[124] J.H. Davis, The description of membrane lipid conformation, order and dynamics by ^{2}H-NMR, Biochim. Biophys. Acta 737 (1983) 117–171.
[125] R.Y. Dong, Deuterium quadrupole splittings and hydrocarbon chain ordering in model membranes, Can. J. Phys. 56 (1978) 678–680.
[126] J.-P. Douliez, A. Léonard, E.J. Dufourc, Restatement of order parameters in biomembranes: calculation of C–C bond order parameters from C–D quadrupolar splittings, Biophys. J. 68 (1995) 1727–1739.
[127] H.U. Gally, G. Pluschke, P. Overath, J. Seelig, Structure of *Escherichia coli* membranes. Glycerol auxotrophs as a tool for the analysis of the phospholipid head-group region by deuterium magnetic resonance, Biochemistry 20 (1981) 1826–1831.
[128] J. Seelig, A. Seelig, Deuterium magnetic resonance studies of phospholipid bilayer, Biochem. Biophys. Res. Commun. 57 (1974) 406–411.

[129] A. Seelig, J. Seelig, The dynamic structure of fatty acyl chains in a phospholipid bilayer measured by deuterium magnetic resonane, Biochemistry 13 (1974) 4839–4844.
[130] A. Seelig, J. Seelig, Bilayers of dipalmitoyl-3-*sn*-phosphatidylcholine conformational differences between the fatty acyl chain, Biochim. Biophys. Acta 406 (1975) 1–5.
[131] J. Seelig, H.-U. Gally, R. Wohlgemuth, Orientation and flexibility of the choline head group in phosphatidylcholine bilayer, Biochim. Biophys. Acta 467 (1977) 109–119.
[132] J. Seelig, Deuterium magnetic resonance: theory and application to lipid membrane, Quart. Rev. Biophys. 10 (1977) 353–418.
[133] J. Seelig, A. Seelig, Lipid conformation in model membranes and biological membrane, Quart. Rev. Biophys. 13 (1980) 19–61.
[134] D.P. Tieleman, S.J. Marrink, H.J.C. Berendsen, A computer perspective of membranes: molecular dynamics studies of lipid bilayers system, Biochim. Biophys. Acta 1331 (1997) 235–270.
[135] D. Poger, W.F. van Gunsteren, A.E. Mark, A new force field for simulating phosphatidylcholine bilayer, J. Comput. Chem. 31 (2009) 1117–1125.
[136] T. Lenné, G. Bryant, R. Holcomb, K.L. Koster, How much solute is needed to inhibit the fluid to gel membrane phase transition at low hydration, Biochim. Biophys. Acta 1768 (2007) 1019–1022.
[137] R. Baron, W.F. van Gunsteren, P.H. Hünenberger, Estimating the configurational entropy from molecular dynamics simulations: anharmonicity and correlation corrections to the quasi-harmonic approximation, Trends Phys. Chem. 11 (2006) 87–122.